



HIGHLIGHTED PAPER

Directed energy deposition (DED) additive manufacturing: Physical characteristics, defects, challenges and applications

David Svetlizky ¹, Mitun Das ^{1,†}, Baolong Zheng ², Alexandra L. Vyatskikh ²,
 Susmita Bose ³, Amit Bandyopadhyay ³, Julie M. Schoenung ², Enrique J. Lavernia ²,
 Noam Eliaz ^{1,*}

¹ Department of Materials Science and Engineering, Tel-Aviv University, Ramat Aviv, Tel Aviv 6997801, Israel

² Department of Materials Science and Engineering, University of California, Irvine, CA 92697-2575, USA

³ School of Mechanical and Materials Engineering, Washington State University, Pullman, WA 99164-2920, USA

Directed energy deposition (DED) is a branch of additive manufacturing (AM) processes in which a feedstock material in the form of powder or wire is delivered to a substrate on which an energy source such as laser beam, electron beam, or plasma/electric arc is simultaneously focused, thus forming a small melt pool and continuously depositing material, layer by layer. DED has several unique advantages compared to other AM processes, such as site-specific deposition and repair, alloy design, and three-dimensional printing of complex shapes. Herein, recent advances as well as the main aspects governing laser-material interactions during the DED process, melt pool thermal behavior, advanced *in situ* monitoring, and interaction mechanisms are critically reviewed. The most critical processing variables and their influence on the deposited material properties, along with defect formation mechanisms and characterization techniques, are also identified and discussed. An overview of high-end applications, current challenges associated with DED processing, and a critical outlook of the technology are presented.

Keywords: Additive manufacturing (AM); Directed energy deposition (DED); Laser Engineered Net Shaping (LENS™); Laser-material interaction; Defects

Introduction

Additive manufacturing (AM), also known as three-dimensional (3D) printing, has been identified as one of twelve disruptive technologies that comprise the fourth industrial revolution (Industry 4.0) [1]. In 2013, GE Aviation adopted metal AM for their production line [2]. In 2018, GE Aviation already produced over 23,000 flight-quality additive parts and targeted to manufacture 100,000 parts by 2020 [3]. The metals AM market [4] has grown in recent years much faster than either the polymers

or ceramics [5] segments. By 2027, the aerospace, automotive, and energy sectors may capture 52% of the total metals AM revenues [5]. It is expected that AM-based repair will come up as an actual application along with new manufacturing technologies.

Powder bed fusion (PBF) and directed energy deposition (DED) are two important AM processes [6] capable of producing fully dense metallic parts for different industrial applications [7,8]. Their different powder delivery mechanisms affect part complexity, support requirements, flexibility of material usage, and surface roughness of the as-deposited part. In 2019, the revenue market shares of PBF and DED systems with respect to the metal AM market were 85% and 8.3%, respectively [9]. It is anticipated that in the next five years, the revenue share of DED technologies will increase to 11.1% while PBF will decrease to 63%

* Corresponding author.

E-mail addresses: Svetlizky, D. (dsvetlizky@gmail.com), Zheng, B. (baolongz@uci.edu), Vyatskikh, A.L. (avyatski@uci.edu), Bose, S. (sbose@wsu.edu), Bandyopadhyay, A. (amitband@wsu.edu), Schoenung, J.M. (julie.schoenung@uci.edu), Eliaz, N. (neliaz@tau.ac.il).

† Permanent address: Bioceramics and Coating Division, CSIR – Central Glass & Ceramic Research Institute, Kolkata 700032, India.

[9]. In another report, it was predicted that the market for DED would reach almost \$755M by 2025 [10]. The leading manufacturers of DED systems with powder feedstock and laser energy source include Optomec®, Inc., Trumpf, BeAM, FormAlloy, DMG MORI, InssTek, Inc., and Nanjing Zhongke Raycham Laser Technology Co., Ltd.. Manufacturers of DED systems with wire feedstock include GKN Additive and Mazak (laser energy source); WAAM, Norsk Titanium AS, Gefertec GmbH, Prodways Tech, and Lincoln Electric (plasma/electric arc); Sciaky, Inc., and Eovo-beam GmbH (electron beam). It was the Sandia National Laboratories that licensed in 1997 the technology of Laser Engineered Net Shaping (LENS™), one of the first commercialized DED processes, to Optomec®, Inc. (Albuquerque, NM) [11].

The quality and properties of parts manufactured by DED depend on (i) the type of DED technology (including the types of feedstock and heat source); (ii) the build environment (vacuum, inert gas, or ambient); (iii) beam-material interactions; (iv) deposition parameters (mainly, laser powder, laser scan speed, hatch spacing, powder feed rate, laser scan strategy); and (v) feedstock attributes. Besides, DED deposited parts are exposed to rapid and repeated heating–cooling cycles during a layer-by-layer deposition that can create unique microstructural features, non-equilibrium phases, solidification cracking, directional solidification, residual stresses, porosity, delamination, and warpage. In general, DED samples often exhibit anisotropy in mechanical properties and heterogeneous microstructures due to the deposition's directional nature. Thus, the thermal history of DED processes controls both the macrostructure and microstructure, which might influence the mechanical properties of as-deposited parts. Some of the defects associated with metal AM can be eliminated, or at least significantly reduced, by process optimization, *in situ* monitoring, and feedback control, thus achieving superior component quality.

Several broad-spectrum reviews have been published on metal AM (e.g., [12–16]) focusing on AM technologies, applications, and/or materials, while only a few have been dedicated to DED technologies [17–26]. These are focused on thermal and fluidic phenomena, process parameter maps, optimization and control, mechanical behavior, and applications. In recent years, significant development is occurring with DED technology in alloy design, repair of critical structures, and bimetallic/multi-material structures. The present review is focused on laser–material interactions, DED's most critical processing variables, and defects formation and characterization in the deposited material. A more concise summary of the principles, advantages, disadvantages, and applications of DED, as well as a brief discussion of current challenges and future directions, are also provided for completeness.

Directed energy deposition (DED) – principles, advantages, and disadvantages

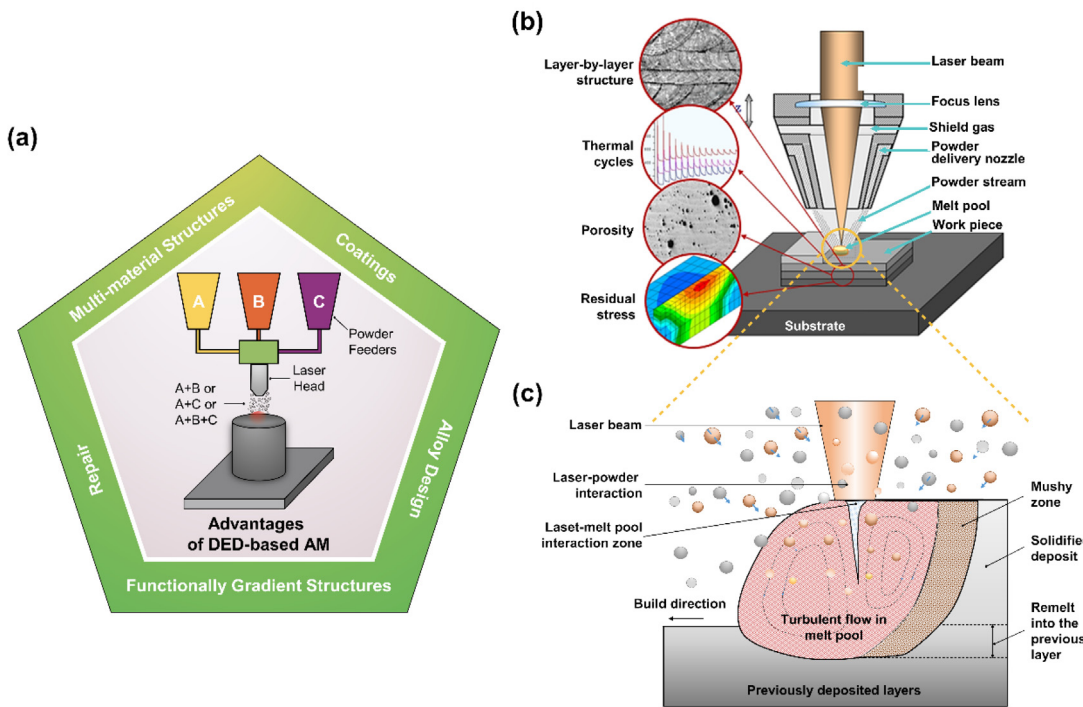
This section briefly summarizes the general principles of DED and its advantages and disadvantages, mainly as compared to PBF. These two processes are complementary, not competing, with DED having major advantages in high-throughput new material development and processing of multi-materials on the one hand, and rapid manufacturing of large near-net-shape parts

with good mechanical properties on the other hand. A concise comparison is also made between DED processes with either different heat sources or different material feedstocks.

DED is an AM process that is highly adapted for deposition of high-performance materials such as stainless steels, tool steels, alloy steels, titanium-based alloys, cobalt-based alloys, nickel-based alloys, aluminum alloys, high-entropy alloys, intermetallics, shape memory alloys (SMAs), ceramics, composites, and functionally graded materials (FGMs) [27]. DED uses a high energy density heat source (laser, electron beam, or plasma/electric arc) that is focused on the substrate, forming a small melt pool and simultaneously melting the feedstock material delivered into the melt pool in the form of either powder or wire [25,27–29]. As the heating source moves forward, the deposited metal solidifies on the substrate, forming a metal track. The metal tracks overlap each other based on the pre-defined hatch spacing (i.e., the distance between successive metal tracks). After completing a layer, the deposition head and the feedstock delivery system move upward by a small distance (slice thickness) to deposit the next layer (Fig. 1b). Thus, deposition of all layers produces a 3D near-net-shape component, similar to the computer-aided design (CAD) model. Before deposition, the 3D digital model is sliced using software to specify slice thickness, hatch spacing, and the deposition path in each layer. Table 1 compares DED processes with different heat sources with respect to some selection criteria [30]. Table 2 compares some characteristics of powder feedstock versus wire feedstock DED.

Based on the energy source and type of feedstock, commercially available technologies are referred to as laser metal deposition (LMD), direct metal deposition (DMD), laser solid forming (LSF), LENS™, directed light fabrication (DLF), electron beam additive manufacturing (EBAM®), or wire plus arc additive manufacturing (WAAM) [29,31]. Some DED technologies such as LENS, DLF, and EBAM deposit the metal in a closed chamber with either a controlled atmosphere glove box or under vacuum, whereas DMD and WAAM use controlled inert gas shroud to prevent oxidation of the deposit. Some DED systems can deposit multiple materials simultaneously and allow the multiple-axis deposition to process reasonably complex geometries. DED is also a useful technique for filling cracks, retrofitting manufactured parts, and repairing high-value metal parts [21,22,32]. DED is capable of depositing large volumes of materials very fast (typically, from 0.5 kg/h for LENS [33] to 10 kg/h for WAAM [34]) and with huge work envelopes (e.g., 6 × 1.4 × 1.4 m for existing commercial printers) [33].

Some international standards are already available for DED processes [30,35]. ASTM 3413 [30] lists the following advantages of the DED process: (1) a broad range of feedstock materials; (2) multi-materials, composites and FGMS can be processed; (3) often better static and dynamic mechanical properties in the as-deposited condition than in PBF-deposited parts; (4) part characteristics can be adjusted locally; (5) printing either full parts or local features, coatings, or repair in a single machine; (6) high deposition rates; (7) larger parts possible compared to PBF; (7) design freedom is typically high relative to conventional manufacturing processes; (8) high technology readiness level (TRL) or manufacturing readiness level (MRL) compared to some other AM processes; (9) some DED machines are hybrid, namely they

**FIGURE 1**

(a) Schematic of DED's critical advantages over PBF from materials design to repair to applications. (b) Microstructure, multiple interfaces, thermal cycling, defects, and residual stress, and (c) interaction among injected powder, laser beam, and melt pool in DED, which in some cases results in keyhole formation in the melt pool. (b) and (c) reprinted from Ref. [37], with permission from Elsevier.

TABLE 1

Comparison between DED processes with different heat sources [30]. Build volume refers to the relative size of components that can be processed by the subject process. Detail resolution refers to the ability of the process to create small features. Deposition rate refers to the rate at which a given mass of product can be produced. Coupling efficiency refers to the efficiency of energy transfer from the energy source to the substrate, and Potential for contamination refers to the potential to entrain dirt, gas, and other possible contaminants within the part.

| Heat source | Build volume | Detail resolution | Deposition rate | Coupling efficiency | Potential for contamination |
|---------------------|--------------|-------------------|-----------------|---------------------|-----------------------------|
| Laser | 3 | 2 | 2 | 1 | 3 |
| Electron beam | 4 | 1 | 3 | 4 | 4 |
| Plasma/electric arc | 3 | 1 | 3 | 4 | 2 |

* Comment: 1 is the lowest, and 4 is the highest.

allow additive-subtractive manufacturing [36]; (10) AM on non-horizontal surfaces is possible; (11) larger powder particle sizes are used in DED with laser compared to PBF with laser (both cost and safety advantages); (12) in-space printing in zero-gravity environment is possible when using DED systems with wire-feed, electron beam energy source, and vacuum chamber.

DED processes suffer from the following disadvantages: (1) shrinkage, residual stress, and deformation can occur due to local temperature differences; (2) they have a lower-dimensional resolution (and sometimes accuracy) compared to PBF with a laser beam, with larger surface waviness; (3) in blown powder systems, higher surface roughness is obtained compared to laser-beam PBF; (4) complexity of parts might be limited, in particular in machines confined to three degrees of freedom; (5) post-fabrication machining is often required; (6) lower powder efficiency and powder recyclability compared to PBF, in particular when printing a mixture of powders. Fig. 1a shows the schematic of DED's critical advantages over PBF from materials design to

repair to applications. Research areas involving advanced materials design to applications in structural, functional, and biomedical areas can only be catered using the DED-based metal and multi-material AM.

Applications of DED

After introducing DED and its pros and cons, this section highlights some existing and emerging unique applications of DED in alloy design and multi-material structures, manufacturing of large structures, repair, and coatings.

Since the commercialization of DED technology in the mid-1990 s, its unique capabilities have enabled applications in several areas apart from printing a 3D structure. Fig. 2 shows a few unique applications of DED technology in manufacturing large structures, repair, and coatings [38–43]. Repair of large, high-value metal parts is a common practice industrially, where welding is typically used, followed by surface finishing. However, for large and/or expensive parts, DED technology can repair the

TABLE 2

Powder feedstock vs. wire feedstock DED processes.

| Parameter | Powder | Wire |
|--|--------|----------------|
| Deposition rate | ✓ | ✓ ¹ |
| Feedstock material variety | ✓ | ✓ |
| Feedstock material cost | ✓ | ✓ ² |
| Machine cost | ✓ | ✓ ² |
| Safety | ✓ | ✓ |
| Power efficiency | ✓ | ✓ ³ |
| Feedstock capture efficiency | ✓ | ✓ ⁴ |
| Larger part sizes | ✓ | ✓ |
| Higher energy input required to melt feedstock | ✓ | ✓ |
| Lower porosity | ✓ | ✓ |
| Operation in zero gravity | ✓ | ✓ |
| Higher resolution | ✓ | ✓ |
| More complex geometry | ✓ | ✓ |
| Printing multi-materials | ✓ | ✓ |
| Surface finish | ✓ | ✓ |
| Dimensional accuracy | ✓ | ✓ |

¹ Similar deposition rates can be achieved with laser-powder, laser-wire, and e-beam-wire; higher rates are achievable with arc-wire.

² Arc-wire systems are the cheapest.

³ e-beam and arc systems have the highest power efficiency.

⁴ ~100%.

structures and add material during repair to minimize future erosion or damage (Fig. 2b) [38]. This is done using a computer-controlled deposition head in DED to deposit material based on the CAD file of the part being repaired. First, the part is analyzed for common areas of damage, for example, thermal degradation or wear, and then a higher hardness or high-temperature resistant material that is compatible with the base alloy is deposited in target locations. Since DED is a melt-cast process, good metallurgical bonding is attained with a diffuse interface. Post-DED heat treatment is sometimes used to reduce residual stresses due to fast cooling rates and high thermal gradients. Finally, surface finishing is done to meet the necessary tolerances. Fig. 2e shows NASA's half-scale, 1.016 m height, RS25 rocket nozzle liner with internal features built in 30 days using laser powder DED to reduce costs and lead times for aerospace applications [39]. Such large metal parts are challenging to manufacture using any other AM technology and are typically large-scale multi-step processes in traditional manufacturing. Fig. 2a shows that LENS™ can be used to repair internal defects in Inconel 718 and other metals. Milling trapezoidal-shaped slots was reported to provide better defect zone preparation for repair than rectangular slots,

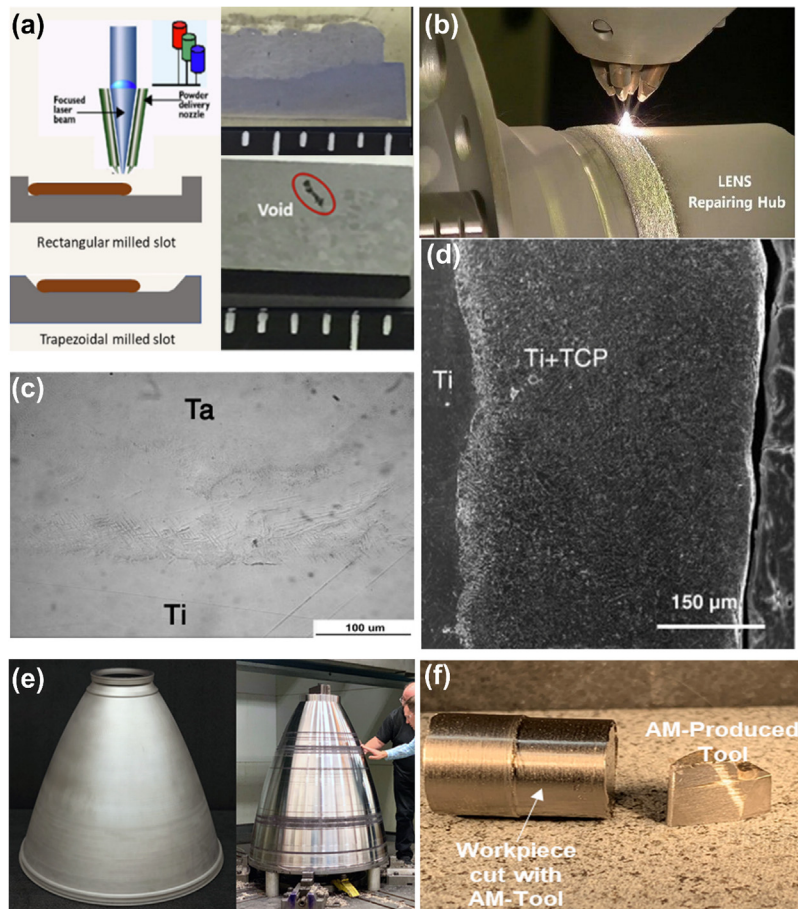


FIGURE 2

DED applications in the manufacturing of large parts, repair, and coatings. (a) Multiple repair and deposition strategies. Reprinted from Ref. [40], with permission from Elsevier. (b) Repair of a large-scale tubular structure [38]. © Copyright Optomec, Inc. (c) Tantalum coating on titanium showing strong bonding in addition to increased bioactivity *in vitro*. Reprinted from Ref. [41], with permission from Elsevier. (d) Calcium phosphate coating on titanium for increased bioactivity. Reprinted from Ref. [42], with permission from Elsevier. (e) A large-scale rocket nozzle manufactured for aerospace applications. Reprinted from Ref. [39], with permission from NASA. (f) Hard coatings of metal carbides with diamond reinforcement for cutting tool applications. Reprinted from Ref. [43], with permission from Elsevier.

while diagonal build direction and heat treatment were found preferable to minimize wear on repaired samples [40]. With a robotically-controlled free axis DED arm, repair of difficult to reach structures such as inside a tube is also possible with deposition of materials along all 360 degrees. Fig. 2c, d, f shows different functional coatings applied to a base material to enhance performance [41–43]. In Fig. 2c, tantalum (Ta) coating is applied on Ti via DED [41]. Tantalum's melting point is very high (>3000 °C), causing traditional processing to be challenging as regular melt-cast processing routes are impossible for Ta. Yet, Ta absorbs the laser energy and has low thermal conductivity, making it easy to melt using laser-based DED. Moreover, Ti and Ta have a complete solid solubility at high temperatures. Thus, Ta coating on Ti was accomplished via DED with excellent metallurgical bonding [41]. Ta-coated Ti also showed good bone cell-material interactions *in vitro*, paving the way to use this technology by applying Ta coatings on metallic implants to improve biocompatibility. In Fig. 2d, a calcium phosphate (CaP) coating is applied via DED on Ti to enhance the implant's osseointegration *in vivo*. Since the Ti-CaP coating material is a metal-ceramic composite, interfacial strength is very high compared to a pure CaP ceramic coating on Ti, the current gold standard in orthopedic and dental implants.

Yet, biocompatibility improvement is nearly the same for Ti-CaP coatings made by DED and conventional pure CaP coatings [42]. Fig. 2f demonstrates DED-processed hard coatings of metal carbides with diamond dust for cutting tool applications [43]. These coatings were free from large-scale cracking, exhibited multiple reinforcing phases, and were found useful in machining of aluminum and AM titanium. All of the abovementioned coatings had been applied to parts manufactured via conventional approaches. However, the novelty of the DED is the ability to deposit on finished surfaces to improve site-specific performance using coatings maintaining strong metallurgical bonding.

Fig. 3 shows two other critical areas of applications for DED processes – alloy design and multi-material structures [44–49]. Alloy design via traditional approaches requires extensive high-temperature capabilities and large amounts of raw materials. Using DED, a large variety of alloys can be deposited in a combinatorial manner under a controlled environment to down-select promising compositions for further analysis in a short period of time. Using a multi-hopper DED system and a programmed powder delivery system, even a single part can be made with varying compositions from one end of the part to the other end, a classic multi-material compositionally graded structure. Such options make a DED machine almost an ideal tool for metallurgists for coming up with structures offering site-specific performances. Fig. 3a shows laser metal deposition (LMD) of blocks consisting of FGM structures of ~500 µm thick layers of Cr-Mo-V hot working tool steel and Ni-based maraging steel [45]. Fig. 3b shows LENS™ deposition of an aluminum alloy block [46]. A recent study showed DED-processed Al 5xxx alloy with altered chemistry from the Al 5083 feedstock to Al 5754 in the as-printed condition due to selective evaporation of Mg, a typical challenge that needs to be accounted for in many systems with alloying elements having varying melting points [44]. Fig. 3c shows high-temperature Cu alloy, GRCop-84, deposited on Inconel 718 with a metallurgically strong interface to enhance the super-

alloy's thermal conductivity. A more than 300% increase in thermal conductivity was reported due to the GRCop-84 layer on 718 alloy [48]. Fig. 3d shows an alternating titanium-niobium carbide structure with different metal and ceramic phases for directional-thermal/structural applications [47]. Such an approach can generate composites in which reinforcements are only placed where they are needed, thus having site-specific properties. Fig. 3e shows LENS™ deposited steel tube with the composition varying from magnetic ferritic stainless steel (SS) 430 to non-magnetic austenitic SS 316 [49]. These examples highlight a few unique areas where the DED technology platform makes a significant difference in manufacturing advanced materials beyond just printing some 3D shapes based on their CAD files.

Current challenges

Although DED technology is growing rapidly worldwide, many scientific and technical challenges need attention to make this technology platform more versatile. The PBF is a more popular metal AM technology platform due to its ability to better tolerances than those achievable in DED. In recent years, hybrid AM (HAM) is becoming popular with DED to meet the tight tolerances in parts. In a HAM system, a DED head is coupled with a computer numerical control (CNC) machining center. After depositing a few layers, turning or milling operations are done to meet the tolerances. The final part looks more like machined parts than a typical AM processed part. Although HAM is exciting, since both deposition and machining are done during the same operation, the build time is relatively long. Moreover, extensive CNC programming and process planning are needed for each part based on its geometry and complexity to decide when to machine and when to deposit material. Such complicated operations may require more experience in running a HAM system than a PBF or a DED machine alone. Additionally, in a HAM system, metal chips from machining can get mixed with the excess powders from the deposition head and cause more material loss from each build operation.

Similarly, for a multi-material part, depending on the deposition head, typically 20–75% of the blown powder is captured in the actual part, while the remaining powder is scattered on the deposition tray. Separation of such mixed powders can be quite challenging, increasing the powder waste and DED operation cost. To avoid this problem, sometimes pre-mixed powders are preferred instead of on the fly mixing for DED operation where unused powders can be collected to reduce starting powder waste.

In this regard, it is essential to note that the powder's recyclability is also an issue in DED. How many times starting powders can be reused or mixed with fresh powders or what happens to the powders' flowability after running through the DED operation are all critical questions that require elaboration. Metallurgical compatibility is another critical factor that needs a more in-depth understanding to move DED for manufacturing multi-material parts. Like other metal AM processes, DED involves fast cooling rates and is controlled by non-equilibrium thermodynamics and related kinetics. Therefore, standard phase diagrams, which are developed using equilibrium thermodynamics, have limited applicability in DED. Naturally, printing multi-material

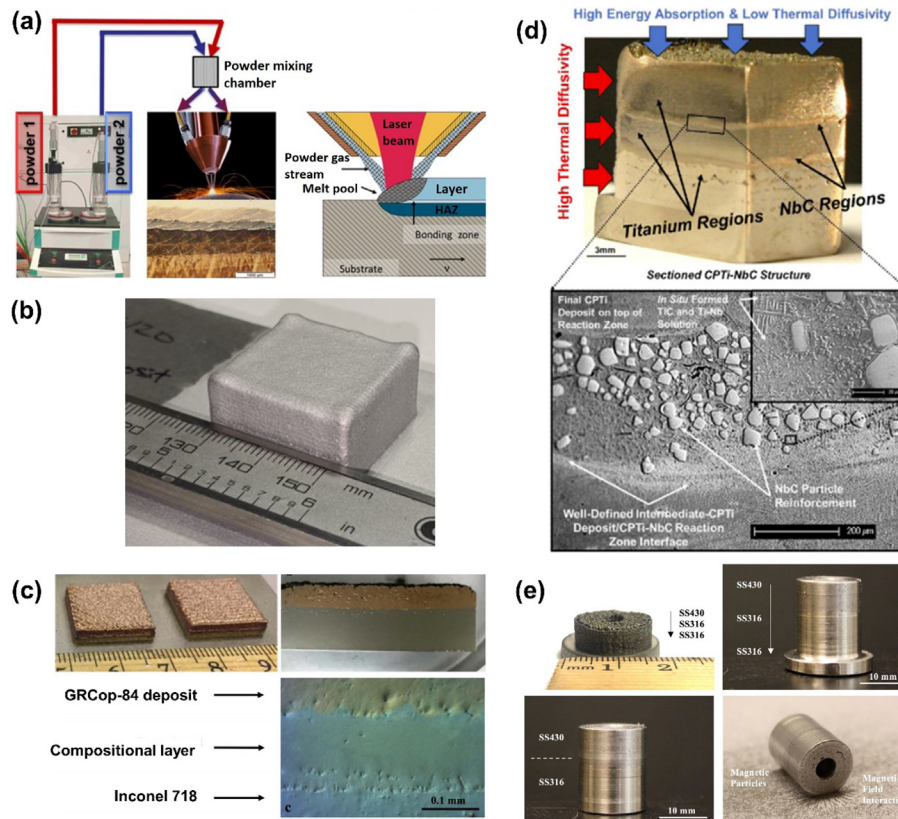


FIGURE 3

DED applications in alloy design and multi-material structures. (a) A concept of processing multi-material structures using DED. Reprinted with permission from John Wiley and Sons: Steel Research International [45], © 2016 WILEY-VCH Verlag GmbH & Co. KGaA, Weinheim. (b) Compositionally designed aluminum alloy block with >99% relative density [46]. © Copyright Optomec, Inc. (c) A bimetallic structure composed of Inconel 718 and GR-Cop84 (copper alloy) processed via LENSTM showing increased thermal conductivity in rocket-nozzle walls. Reprinted from Ref. [48], with permission from Elsevier. (d) Alternating titanium-niobium carbide structure with different metal and ceramic regions for directional-thermal/structural applications. Reprinted from Ref. [47], with permission from Elsevier. (e) Bimetallic stainless-steel structure processed using LENSTM showing distinct regions of magnetic (430SS) and non-magnetic (316SS) steels. Reprinted from Ref. [49], with permission from Elsevier.

structures may require extensive trial-and-error type experiments to identify the processing windows where all compositions can be deposited without cracking and other defects.

Predictive capability using computational materials science, advanced machine learning methods, and *in situ* monitoring and adaptive control techniques involving physical, chemical, and thermal properties of different alloys will be advantageous in the coming years to establish metallurgical compatibility for manufacturing monolithic and multi-material parts. Some of the other issues are more related to DED machines. For example, most DED deposition heads have three axes of freedom. However, a machine with a 5-axis or a free-axis deposition head opens the possibility of manufacturing a wider variety of additional structures or repairability with more complex geometries. Similarly, most DED systems employ a 500 W or a 1000 W lasers as the heat source. Although higher power lasers can increase printing speed, there may be a compromise with part resolution in high laser power machines. And finally, although most DED operations use metal powders as the feedstock material, the cheaper wire-feed DEDs are also available. Metal wires are significantly cheaper than metal powders, and wires are safer and easier to store than powders. However, melting metal wires

require higher laser power, which makes wire-feed DED systems more expensive.

Laser–material interactions

To properly understand and eventually control the DED's thermal environment, it is necessary to understand the underlying laser beam-powder-melt pool (LB-P-MP) interactions. Fundamental understanding of the underlying mechanisms that govern DED will facilitate proper adaptive control of the ensuing microstructure, residual stresses, and defects, with the ultimate goal of optimizing material properties and performance. This section reviews related aspects, such as inflight powder particle heating, spatial and temporal thermal fields present in the melt pool, particles-melt pool interactions, and their monitoring *in situ*. A brief discussion of heat source-wire interactions is also included, although this area lags behind the powders' equivalent.

Laser powder-based DED involves powder delivery at a pre-selected and controlled rate using an inert gas as a carrier media. The powder is directed towards the melt pool via a series of nozzles. The powder flow acquires a conical geometry as it emerges from the nozzles and travels towards a melt pool [50,51]. The concentric powder streams converge as they approach the melt

pool, leading to inter-particle collisions as well as LB-P-MP interactions. Heating, melting, vaporization, and solidification all occur during DED. As such, deposited materials are typically characterized by a layered structure, experience multiple thermal cycles, and generally contain pores and residual stresses, as shown in Fig. 1b [37]. In the region adjacent to the melt pool, injected powder particles interact with both the laser beam and the melt pool, as illustrated in Fig. 1c. Convective turbulent flow is associated with the melt pool, and in some cases, deposition conditions lead to the formation of a 'keyhole,' which originates from the metal vapor that is sometimes created when a material is processed using conditions involving very high laser beam intensities.

These phenomena are critically dependent on the thermal and physical properties of the material being deposited and on process parameters, including laser power and intensity profile, powder flow rate, velocity and trajectory, and the scan geometry and frequency of laser pass, for example. Therefore, much ongoing research aims to establish a fundamental understanding of the underlying mechanisms that govern DED to properly exercise adaptive control over the ensuing microstructure, residual stresses, and defects with the ultimate goal of optimizing material properties and performance.

Inflight particle heating

The injected powder particles emerge from the nozzle and interact with the laser beam. Depending on the process conditions and the local power density, the powders simultaneously attenuate the laser beam and absorb thermal energy. As a result, powder particles are heated and possibly melted as they travel towards the substrate's surface, depending on the thermal and momentum fields present [51,52]. An example of a thermal image of powder particles interacting with a laser beam is shown in Fig. 4a. The geometrical relations illustrated in Fig. 4b show how trajectory and incidence angle can affect temperature as particles arrive at the melt pool [52]. The amount of thermal energy absorbed by the powder particles as they travel towards the melt pool depends on the particle density and the associated thermo-physical properties, as well as on particle morphology and size distribution; the residence time in the laser beam and the gas velocity also affect the transfer of thermal energy [53].

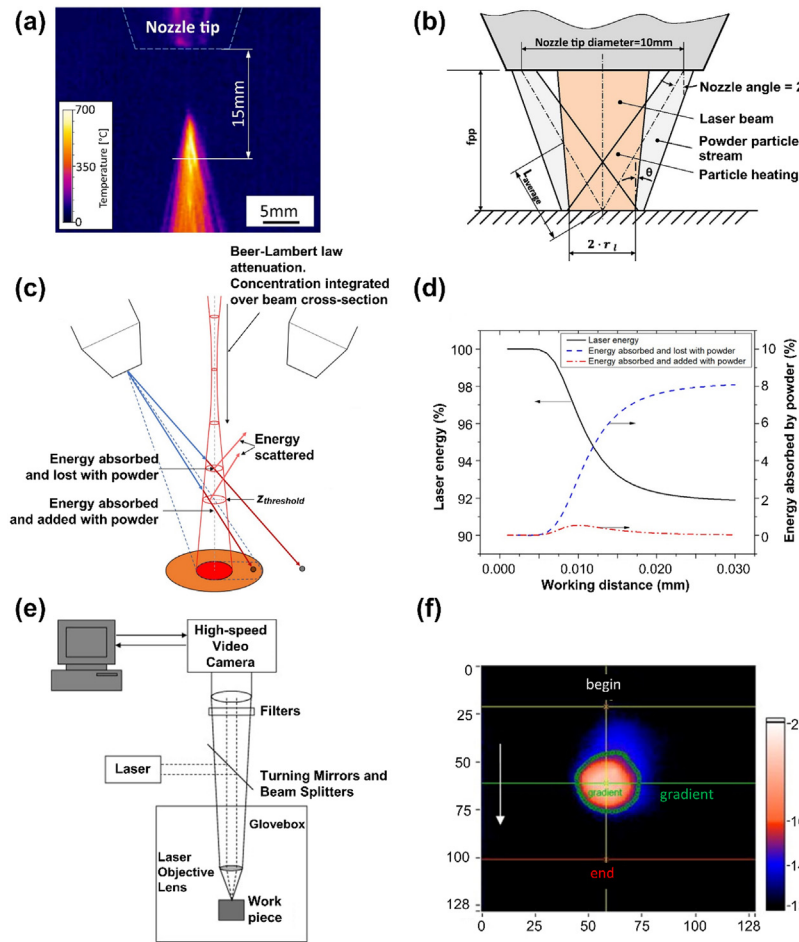
In a related study, the partitioning of energy during DED was investigated in detail for the particular case of 316L SS powder and an Nd:YAG laser [54]. The numerical and experimental results indicated that the substrate absorbed 30% of the laser power and reflected approximately 54%; the powder reflected 11%, 4% was lost due to dispersed powder, and notably, only 1% was absorbed by the deposited powder. Similar results were reported in another study on the influence of powder trajectories and residence time within a laser beam [55].

The partitioning of laser energy during DED deposition is also closely related to the working distance (WD), defined as the distance from the nozzle plane to the deposited material's surface. During the deposition, the WD converges to an equilibrium value, critically influenced by thermal energy accumulation, initially in the powder mass and eventually in the deposited material. The energy that is absorbed by the powder is transferred into the melt pool as the powder is deposited or is dissipated into the

environmental chamber if the powder is diverted away from the melt pool, as illustrated in Fig. 4c, d. To properly understand and eventually control DED's thermal environment, it is necessary to fully understand the underlying LB-P-MP interactions. However, this remains a formidable challenge, given the melt pool's small size, large thermal gradients, and the solid/liquid interface's fast movement. For example, when the feedstock powder experiences a high temperature before impingement onto the melt pool, the localized deformation during impact and its associated temperature variation and microstructure will differ, depending on the local position in the melt pool. High-speed photography and thermal imaging, along with numerical simulations, are essential tools that can be used to characterize the attenuation effects that particles have on the laser beam, particle melting, and particle-pool interaction behavior during the DED process, while high-speed thermal imaging provides detailed information related to the thermal behavior (namely, thermal gradients and cooling rates) in the vicinity of the melt pool.

Thermal behavior of the melt pool

The laser beam impinges on the surface of the material being deposited, resulting in a focused and fast-moving melt pool during DED. To properly understand the mechanisms that govern microstructure evolution during DED requires knowledge, not only of the laser beam's interactions with the melt pool but also on the spatial and temporal thermal fields present in the melt pool. Monitoring the thermal-based signatures (e.g., melt pool temperature gradients and cooling rates) during the deposition process allows the prediction of microstructural evolution characteristics (e.g., dendrite arm spacing and grain morphology), mechanical properties (tensile strength and wear resistance), and defect formation (e.g., porosity and cracks). As such, non-contact thermal imaging, such as visible and near-infrared (IR) radiation pyrometry, can be applied to determine the thermal characteristics of the melt pool and the associated cooling rates [56–61]. In a related study, a single-wavelength high-speed digital charge-coupled device (CCD) video camera was used to measure the thermal images obtained during DED deposition of 316L SS [61]. A 650 nm broad band pass filter and telephoto lens were used to image the deposition path. A measured solidification interface temperature of 1650 K for 316L SS showed that the melt pool size increased with laser power up to 275 W. These results reveal that the cooling rate is $\sim 10^3$ K/s and that the highest cooling rate can be obtained at the lowest power and highest laser scan speed. Another experimental study involving a high-speed digital CCD video camera with a top view of the melt pool was also reported [56,59]. Compared to the experimental arrangement in [61], the camera in these studies was stationary and had the same focal point as the laser. Thus, in this way, the camera was always in focus and could image the melt pool regardless of the x , y , and z locations. The thermal behavior of WC-Co cermet was studied during DED using an *in situ* high-speed thermal imaging arrangement (viewed from the top) (see Fig. 4e and f), in combination with finite element analysis (FEA) [56], to provide fundamental insight into the factors that influence microstructure evolution. The image is shown in color to show the temperature in degrees Kelvin, while values on the x - and y -axes show

**FIGURE 4**

(a) Thermal image of the heated powder particles at the nozzle exit for a 1000 W laser power, and (b) geometric relations. Reprinted from Ref. [52], with permission from Elsevier. (c and d) According to the Beer-Lambert law and powder spray pattern, energy partitioning as the laser is absorbed and scattered by powder in flight. Reprinted from Ref. [51], with permission from Elsevier. (e) Experimental arrangement showing a thermal measurement system positioned above the DED system, and (f) a thermal image of a WC-Co sample looking from the top when layer 5 was deposited. Reprinted from Ref. [56], with permission from Elsevier.

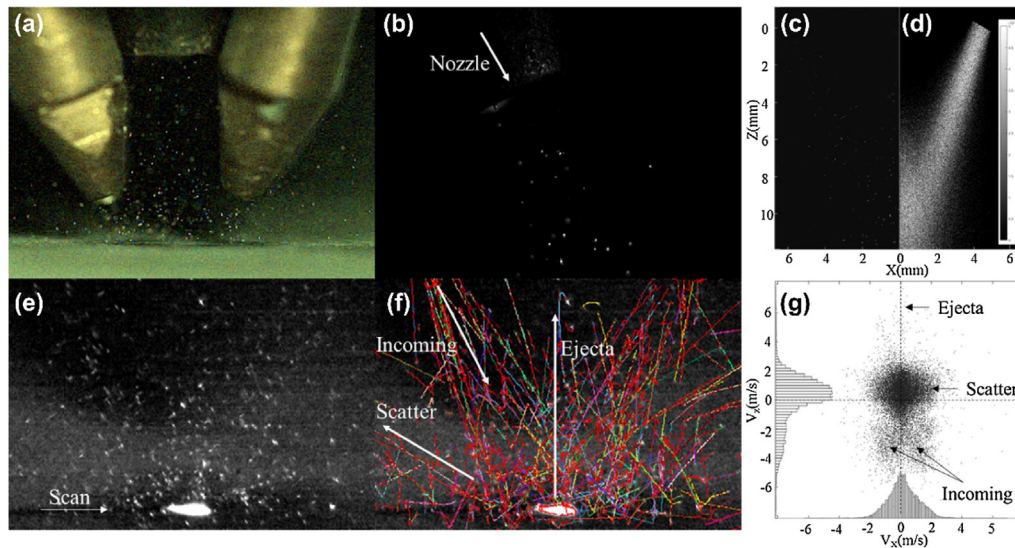
the pixel's image size. The white arrow illustrates the traverse direction of the laser beam. The *in situ* high-speed thermal imaging can be applied to quantify the thermal gradients and cooling rates in the region close to the melt pool, whereas the 3D FEA is implemented to cover the entire deposited region. In the case of non-rebounding particles traveling through the laser beam, there is a threshold z-height below which particles will become immersed in the pool and above which the particles will completely miss the melt pool [51].

A two-wavelength pyrometer, another thermal imaging system, has received attention for the study of DED processes mainly because it uses the ratio of radiation's relative intensities at two different wavelengths. One benefit of this approach is that it is independent of an absolute emissivity value, thus providing a more accurate temperature measurement [60], with a margin of error reportedly between ± 6 °C. The thermal behavior of DED-processed 316L SS was investigated [60] with an imaging pyrometer recording within a dynamic range from 1500 to 2500 K. The thermal gradient and cooling rate in the melt pool and the surrounding region were derived from the temperature profile,

showing that the temperature gradient from the center of the pool is on the order of $10^2 \sim 10^3$ K/mm, and that the cooling rate is on the order of $10^2 \sim 10^4$ K/s in the DED processed zone. One limitation of the thermal imaging methods is their inability to acquire the entire thermal history of deposited components, especially the solidified materials' temperature variation.

Particles–melt pool interactions

In situ monitoring can provide crucial information on the influence of process parameters on powder flow, including laser-melt pool interactions, laser-particle interactions, melt pool dynamics, and pore formation. A recent study using a high-speed camera was carried out to measure the interactions between particles in flight and with the melt pool [62]; this study generated helpful information to analyze and understand particle melting and particle-pool interactions DED process. Fig. 5 shows several frames that reveal notable details as the powder particles travel and impinge on the melt pool [62]. The results reveal individual powders arriving at the melt's surface, leading to the formation of ripples. These particles remained on the surface for

**FIGURE 5**

Powder flow (a) from the front of the nozzles to the substrate, (b) from one nozzle to capture particle velocities, (c) lower speed video (10 kHz) provides (d) a one million particle dataset to identify spatial concentration of the spray, (e) flight during single track deposition, (f) respective particle trajectory tracking, and velocity components plotted in (g). Reprinted from Ref. [62], with permission from Elsevier.

~0–600 μ s before being absorbed into the melt. In some cases, particles bounced away from the surface after interacting with particles already present on the surface. To provide statistical information on the particles' velocity profiles, powder trajectories were traced from the high-speed images (Fig. 5f). Moreover, this study also formulated and implemented a three-phase (gas, liquid, solid) computational fluid dynamics (CFD) model to determine the mechanisms that govern particle impact, melt pool dynamics and wettability. The CFD model results were then compared to experimentally obtained results for individual particles of 316L SS [63]. Overall, this study helped establish the influence of material thermophysical properties, residence time, particle size and temperature, impact velocity, melt pool conditions and surface tension during DED.

Cunningham et al. [64] measured single-track laser-materials interactions using a Ti-6Al-4V baseplate in a recent fundamental study. Using *in situ* imaging (Fig. 6a), it was shown that the evolution of vapor depression and keyhole formation depended on input laser energies. It was found that lower laser powers and corresponding input energies tend to decrease the laser's effective drilling rate, reducing the amount of keyholing that occurs.

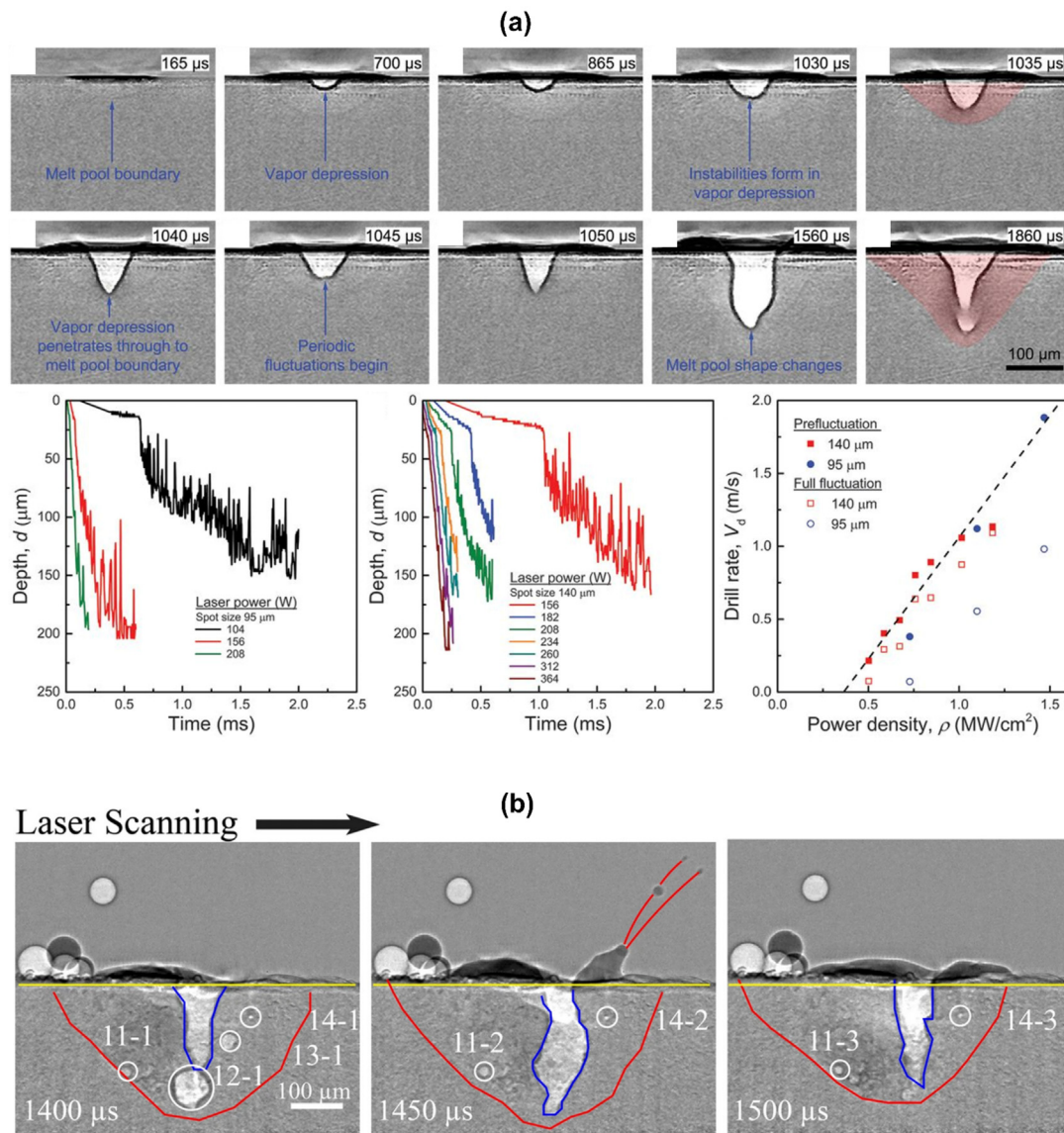
In another study, high-speed X-ray imaging was used to characterize both the powder flow and the laser's interactions with the melt pool [65]. A specially designed DED apparatus was used to image the DED deposition of Ti-6Al-4V powders. Results provide novel insight into the influence of laser-melt pool interactions on porosity formation [65]. Fig. 6b provides interesting detail on the formation of gas pores and pore evolution from a keyhole cavity. The figure also shows that the collapse of a cavity near the bottom of the melt pool leads to a particle's ejection from the surface (i.e., this is described as spattering). Generally, spattering occurs due to the presence of large pressure gradients, or recoil pressure, induced by the vapor-plasma plume and helps stabilize the melt pool during the DED process, potentially lead-

ing to the formation of surface defects or increased surface roughness.

Laser-wire interactions

In laser wire-based DED, a technique based on laser welding with wire filler, the process is also sensitive to the interactions between laser beam and wire. Findings related to laser-matter interactions are not necessarily applicable to both powder-based and wire-based DED processing, given that the two processes are dissimilar. In addition to laser power, traverse speed and wire feed rate, there are additional parameters that influence the interactions between the wire feeder and the laser beam, such as laser/wire or laser/substrate angle, wire tip position relative to the melt pool, wire protrusion distance and feed direction, which require careful tuning [66]. The wire is generally deposited via globular transfer, smooth transfer, or plunging during processing. It is essentially a requirement that the molten wire tip is in physical contact with the melt pool at all times for defect-free deposition.

The closed-loop process monitoring and control with visual sensing and image processing have been developed and implemented for laser wire-based deposition processes to achieve good process stability [66–68]. The interactions between the wire tip and the melt pool during a deposition process can be monitored using a Complementary Metal Oxide Semiconductor (CMOS) camera. The visual feedback helps identify any disturbances and evaluates the controller's efficiency [66]. The time interval between when the wire tip enters the laser beam and when it later enters the melt pool relies on the wire nozzle's position and angle. The wire tip will melt prematurely when exposed to excessive energy, forming droplets of molten wire, leading to the formation of a "weak link" rather than the situation when there is a smooth transfer. If the wire feed rate is too high relative to the melt pool's energy input, the wire might not be appropri-

**FIGURE 6**

(a) Single-track laser experiments (stationary laser) over a Ti-6Al-4V build-plate show the melt pool's evolution and corresponding vapor depression 'keyhole' of a solid material over the time range of 0–1.7 ms. Reprinted from Ref. [64], with permission from the American Association for the Advancement of Science (AAAS). (b) Evolution of cavity, melt pool, porosity, and spattering in a DED simulation experiment with a laser power of 250 W and a scan speed of 100 mm/s. Reprinted from Ref. [65], with permission from Springer Nature.

ately melted, increasing the risk of lack of fusion (LoF) defects. A review of the published literature suggests that research into the fundamental mechanisms that govern the laser beam and wire interactions remains relatively limited and that further work is needed.

Visualization techniques, such as high-speed imaging described above, continue to be improved and provide critical new capabilities that will facilitate an in-depth understanding of some fundamental scientific questions related to laser-material interactions and microstructural evolution during DED materials processing. For instance, what are the mechanisms that govern pore formation and residual stress evolution? We anticipate that new and more sophisticated visualization techniques will continue to evolve and mature, driven by the need to fabricate increasingly complex DED components. Recent examples of

such complexity are provided by recent work on functionally graded composites, directionally solidified components, and non-equilibrium microstructures, which often require unusual combinations of process parameters.

Dominant processing variables in DED

The fabrication of high-quality parts by DED technology is not a straightforward task. The DED process is associated with many processing variables, all of which control the deposit's thermal history and solidification and significantly affect the as-deposited material's microstructure, physical and mechanical properties. In this section, the dominant process parameters that govern the DED process and their influence on the microstructure and behavior of the deposited material are reviewed. In addi-

tion, current and potential techniques for DED process optimization are discussed.

DED processes use a focused heat source in the form of laser beam, electron beam, or plasma/electric arc. Thus, samples prepared with a DED process experience repeated thermal cycling and very high cooling rates of the melt pool (10^3 – 10^5 K/s for laser melting [69]), which upon solidification results in fine, out of equilibrium microstructures with high residual stresses, and in some cases – cracking [70]. For blown-powder DED processes, the process parameters influencing the deposited material are classified into three main branches: (1) system (specifications) dependent, (2) feedstock (powder, in this example) dependent, and (3) process (deposition) variables dependent. These are presented in Fig. 7. The complex thermal history and the high number of the processing parameters listed in Fig. 7 render it difficult to fully characterize and study each parameter's effect (and their crosslinking interactions) on the as-deposited material.

It is worth noting that similar to welding processes, the DED process is highly dependent on distinct properties of the powder

feedstock material, including chemical composition, melting temperature, thermal conductivity, reflectivity, specific heat capacity, melt viscosity, melt surface tension, spectral emissivity, etc. [71]. The high dependence of the material properties on the deposition process results in a need for material-specific process optimization. In recent years, various numerical simulations and *in situ* monitoring techniques accompanied by closed-loop adaptive control were presented to address this challenge, predicting, correlating, and controlling the optimal processing parameters for the deposition of a given material [23,65,71–78]. Fig. 8 shows an example of a schematic workflow simulation of a compositionally graded rocket nozzle processing. Such a model enables determining the optimal process parameters based on a pre-defined geometry and material properties by modeling the deposition processes using modeling the thermal, solidification, microstructural, and performance numerical simulations. Based on the simulated optimal process parameters, the deposition process is executed according to a pre-defined tool path combined with *in situ* monitoring techniques and closed-loop feedback control [79].

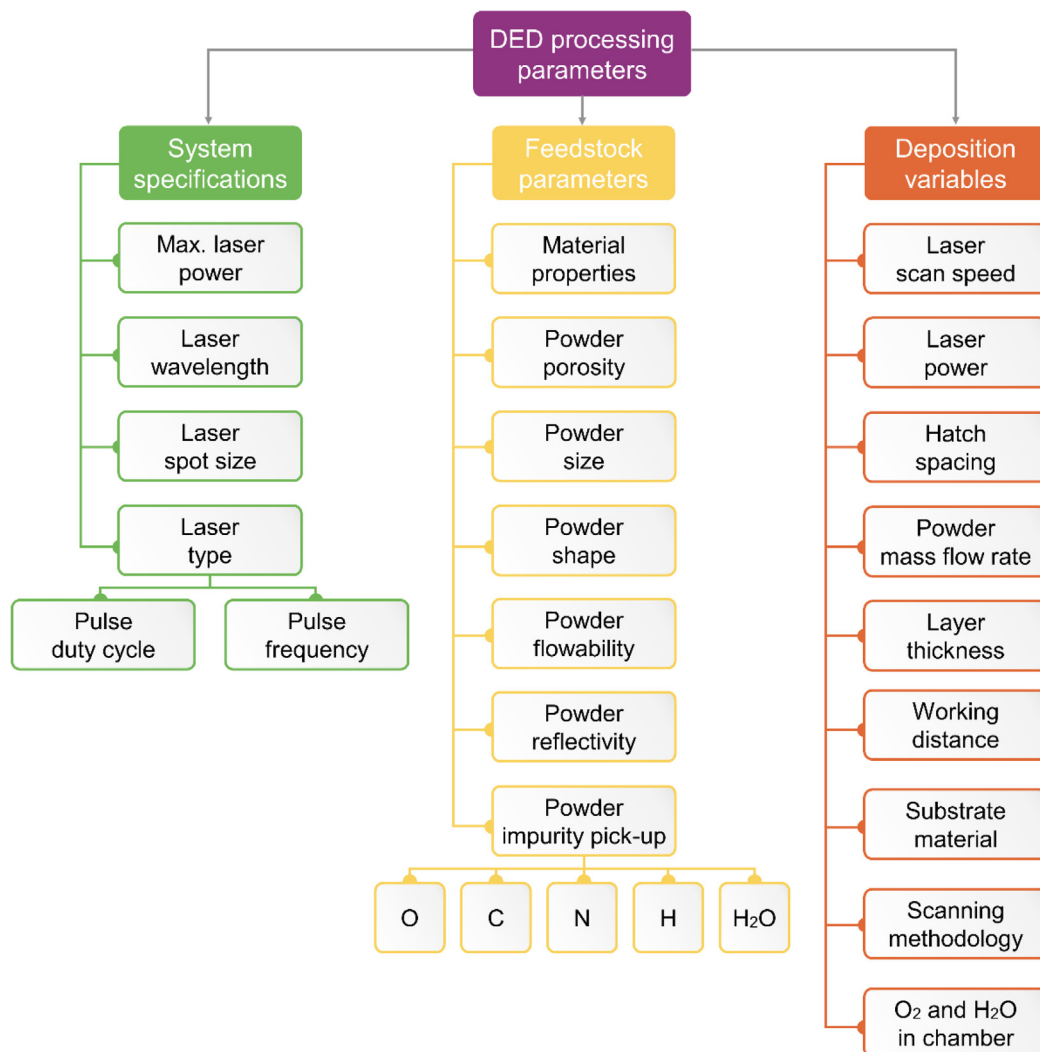
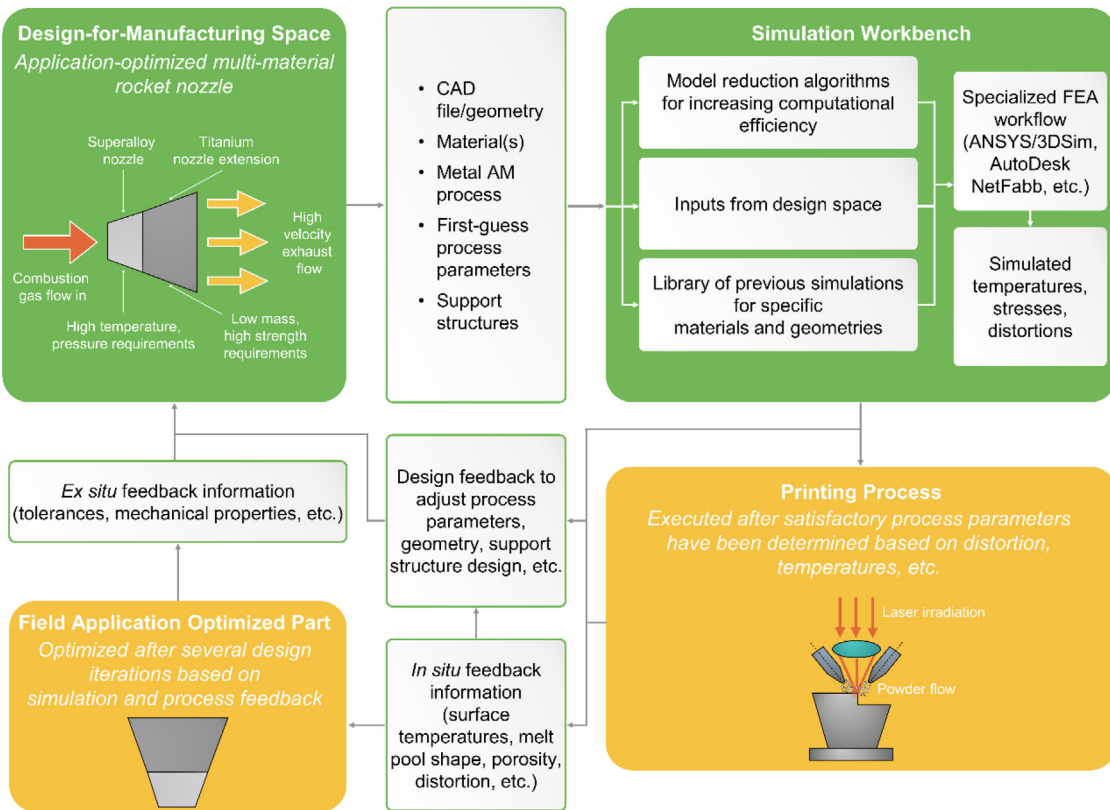


FIGURE 7

DED process parameters diagram.

**FIGURE 8**

Flow chart for DED AM of a critical component combined with FEA simulation, *in situ* monitoring, and feedback control to optimize process variables [79]. Adopted with permission from Elsevier.P

To date, such advanced and complex *in situ* simulation-monitoring-control methods are still considered a big challenge. Among others, the online detection and *in situ* repair of defects formed during part processing (e.g., porosity, LoF defects, distortion, inclusions) and other process signatures (e.g., melt pool geometry and temperature, powder stream distribution, deposit height) with sufficient response time are limiting factors. However, the introduction of advanced adaptive control and *in situ* monitoring techniques based on machine learning algorithms show very promising abilities to optimize the numerous process parameters, perform online process monitoring, and control the process during the deposition process [78,80–82]. Experimental-based process optimization tools, such as the design of experiments (DOE) methods, are considered standard practices. The DED processing parameters and their crosslinking synergistic and antagonistic interactions directly affect the resulting microstructure, mechanical and physical properties of the as-deposited material. Though numerous reports have studied the influence of the DED process-dependent parameters on the as-deposited material properties [83–95], the correlation between the crosslinking interactions has not yet been studied in depth.

The laser power, laser scan speed (also referred to as traverse speed), and powder mass flow rate (PMFR) are considered as three primary DED processing variables in practice [24,29,96–99]. On the other hand, parameters such as hatch spacing, diameter of the energy source, z-step, and working distance are commonly defined as constant throughout the optimization process based on preliminary material-specific experimental data [97,100]. This

is usually achieved by the deposition and analysis of single/double tracks with various sets of processing parameters.

Effective energy density, E (J/mm^2), and powder density, F (g/mm^2), parameters are commonly utilized as factors that express the combination of the dominant processing parameters for correlation with continuous deposition and deposit aspect ratio [101]:

$$E = \frac{P}{vd} \quad (1)$$

where P is the laser power (J/s), v is the laser scan speed (mm/s), and d is the laser beam diameter (mm),

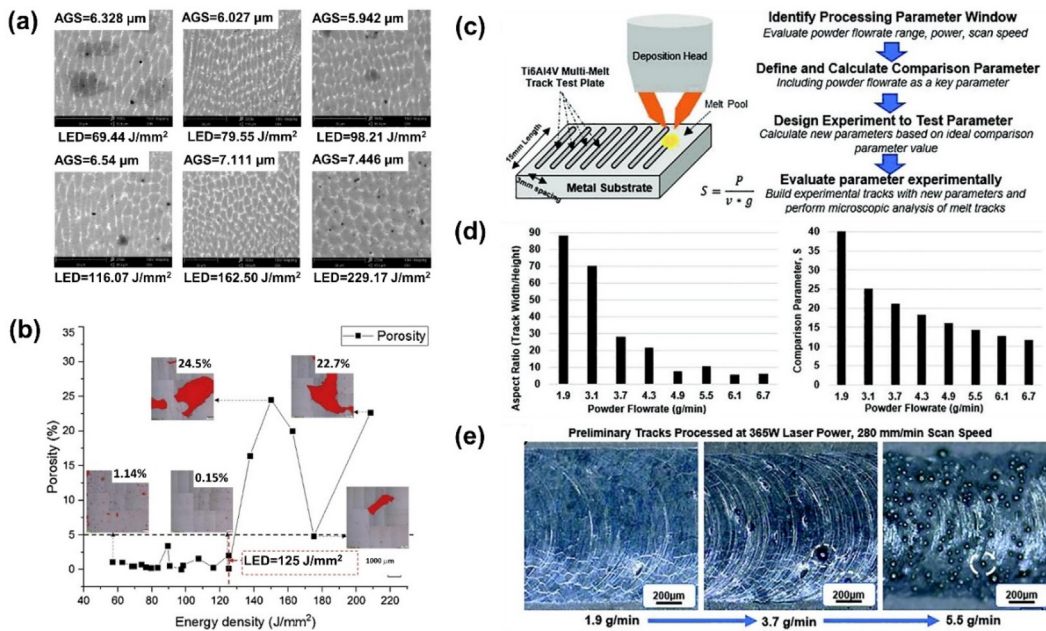
$$F = \frac{G}{vd} \quad (2)$$

where G is the powder mass flow rate (g/s).

Both parameters jointly control the laser's effective residence time and directly affect the melt pool temperature, cooling rate, and the resulting microstructure. Furthermore, the powder flow rate was reported to affect the laser attenuation near the powder's consolidation plane into a single stream, and thus indirectly affect the energy density, too [55]. In a recent study, Traxel et al. [102] showed that a comparison parameter, S , is insightful for DED processes, where S is defined as:

$$S = \frac{P}{vG} \quad (3)$$

The comparison parameter is similar to Simchi's energy input relationship [103]; however, it is more useful for DED processes. In another recent report, DED was employed for the deposition of

**FIGURE 9**

(a) Effect of laser energy density on grain morphology and average grain size (AGS), and (b) porosity of as-deposited Inconel 718. (a and b) reprinted from Ref. [104], with permission from Elsevier. (c) Schematics and workflow of DED processing design using LENS™. (d) Initial deposition tracks with variable powder flow rate, and (e) characteristics of builds at different flow rates. (c–e) Reprinted from Ref. [102], with permission from Elsevier.

Inconel 718 [104]. It was found that the microstructural features like grain morphology, dendritic arm spacing, and porosity (Fig. 9a and b) significantly vary with the applied laser energy density. Compared to its wrought form, the as-deposited Inconel 718 had reduced average grain size and dendritic arm spacing. This was ascribed to the inherent high cooling rates in the DED process. Fig. 9c–e shows the influence of S in multi-track experiments using Ti–6Al–4V. Increasing powder flow rate in S decreases the overall energy input as more mass is delivered to the melt pool, which requires more energy to melt the material [102]. In these experiments, complete melting of particles was selected as the main factor for a quality build. However, all other factors, including aspect ratio and build heights, were viewed as secondary indications. The effect of energy density and powder density on the height of single-layer deposition of AISI M4 tool steel has been reported as well [105]. The results indicated that the deposit's average layer height increases with an increase in both the energy density and the powder density. Furthermore, a linear correlation was observed, allowing to predict the deposit height for a given energy and powder densities.

In the case of DED of Inconel 718, the laser energy density was considered a robust parameter resulting in similar material porosities at similar energy densities [106]. However, a recent report [44] has shown that even with the same energy densities in the DED of Al-Mg alloy, the obtained material density varies. The discrepancies in results show that the specific energy density cannot serve as a single individual robust process parameter, but one should take into account additional factors like feedstock material properties, including laser reflectivity, thermal conductivity, and melt pool surface tension, can directly affect the as-deposited material properties and defect formation. For example, to accomplish a complete melting of Al-based alloy powder, high energy input is required due to its inherently high surface reflectivity [107–109] and high thermal conductivity [110,111]. This

leads to the evolution of a non-stable melt pool and excessive thermal energy accumulation, which might result in defects such as cracks and pores in the as-deposited material [108]. Furthermore, the high laser energy needed to melt such powder may also affect the final composition of the as-deposited material due to the vaporization of low melting point alloying elements such as Mg, Zn, etc. Consequently, such chemical composition variations may affect the resulting microstructure, porosity, mechanical properties, and corrosion resistance. On the other side, insufficient laser energy might result in an inability to properly melt the powder feedstock, causing a balling effect or voids along the circumference [112].

In blown-powder DED processes, the feedstock is delivered into the molten pool through the deposition head nozzles. Thus, the powder mass flow rate is an important parameter that determines the amount of feedstock introduced into the molten pool. However, the amount of material introduced into the molten pool is also determined by the deposition head movement, which is equivalent to laser scan speed. Thus, laser scan speed can control the energy density and the amount of material delivered into the melt pool. Several studies showed that laser scan speed influences the melt pool's solidification behavior [113–115]. Hence, it significantly influences the microstructure and mechanical properties of the deposited material [116]. The combination of powder flow rate and laser scan speed determines the effective residence time of laser per amount of powder introduced into the melt pool [19]. In general terms, increased residence time will increase the volume of powder introduced into the melt pool and the energy input, yielding larger deposits. However, increasing the powder density is not the only parameter that affects powder catchment efficiency. The powder feedstock's catchment efficiency is defined as the powder that is

incorporated and absorbed in the molten pool [116–118]. Physical material properties such as melt pool temperature, surface tension [117,118], and powder flow dispersion characteristics [51,119] may also affect the catchment efficiency, and consequently – the deposit geometrical properties.

The molten pool and deposit geometry evolution in Inconel 718 were studied [120] through 3D numerical simulation accompanied by validation experiments. It was shown that while an increase of the applied laser power does not affect the deposited layer height, it does cause an increase in melt pool width and penetration depth (Fig. 10). This phenomenon was explained by the fact that increased laser power results in increased catchment efficiency due to increased molten pool surface area. Therefore, an increased powder mass is dispersed over a larger melt pool, and thus it has a minor effect on the deposit height.

As DED processing of 3D parts and its unique capabilities such as surface cladding and repair are in increasing demand in high impact industrial applications, efficient process optimization becomes a necessity. However, while numerous studies have tried to describe the mechanisms and effect of the various DED process parameters on the deposited material microstructure, defect formation, and properties, a deep fundamental understanding of the governing mechanisms and the synergistic and antagonistic interactions between them are not yet fully understood.

Defects in the deposited material and their characterization

DED is a non-equilibrium processing technique with fast cooling rates and high thermal gradients. These thermal conditions can

lead to complex phase transformations and microstructural changes, non-uniform residual stresses, and distortions, porosity, cracking, and consequently – degradation in corrosion resistance, mechanical behavior (e.g., ductility and fatigue strength), and premature failure. These are the subject of this section. Formation mechanisms, measurement, modeling and mitigation of these defects are discussed. Table 3 summarizes some of the main defects, their origin, selected effects on the material properties and part, and their characterization techniques. The following subsections discuss them in more detail.

Residual stresses and distortion

Origin of residual stresses: All thermomechanical manufacturing processes inevitably result in formation of residual stresses [121]. Due to DED processes' layer-by-layer nature, the part goes through a highly complex thermal history, including melting, remelting, and reheating the material [27,57,74,122–125]. Fig. 11a shows a model for residual stress formation during the heating and cooling cycles. Fig. 11b shows the *in situ* thermocouple readings during LENS™ deposition of H13 steel box. Each peak represents the thermocouple response as the laser passes over the thermocouple [57]. DED is a non-equilibrium processing technique with fast cooling rates of 10^2 – 10^4 K/s [53,86,124–126] and thermal gradients on the order of 10^4 – 10^5 K/m [57,127] (Fig. 11c and d). This can lead to complicated phase transformations and microstructural changes [124,126]. The residual stresses introduced by AM can be highly non-uniform, both spatially and in the build direction, and often have high gradients of up to $\sim 10^2$ MPa/mm [128,129]. Overall, the key physical factors governing the evolution of residual stresses and distortion

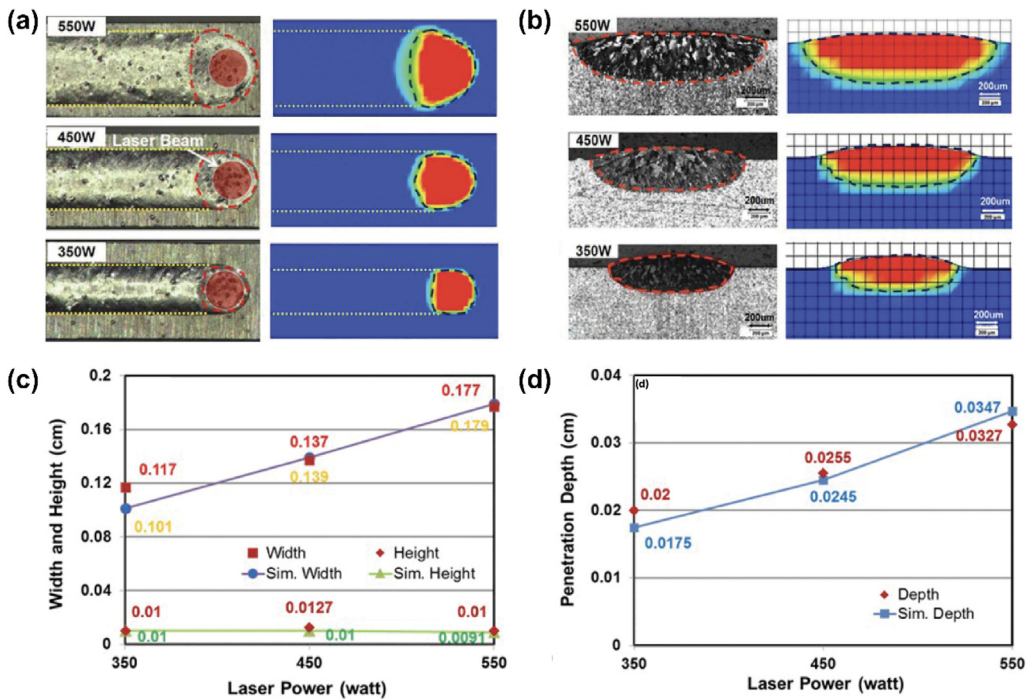


FIGURE 10

Top view (a) and side view (b) of experimental versus simulation single-track deposits at different laser power. The effects of applied laser power on the deposit geometry (c) and penetration depth (d) of Inconel 718. Reproduced from Figs. 8 & 9 in Ref. [120], Welding Journal, August 2014, vol. 93, pp. 292s–300s. © American Welding Society.

TABLE 3**Characteristics of the primary defects in DED-processed materials and their characterization techniques.**

| Defect | Defect's origin | Defect's selected effects on the deposited material properties | Defect's characterization techniques | Mitigation |
|-----------------------------------|--|--|--|--|
| Residual stresses and distortions | High cooling rates and thermal gradients | Induced phase transformations, loss of geometric tolerance, cracking, delamination, degradation in fatigue behavior, premature failure | Hole drilling, serial sectioning, ring-core drilling, X-ray and neutron diffraction, speed of sound, Barkhausen noise, computational models | Substrate preheating, preheating the chamber and printed part during deposition, optimization of the scan strategy, post-print heat and surface treatments |
| Porosity | High laser energy density, feedstock porosity, selective evaporation, entrapment of shielding gas, insufficient energy input (LoF) | Degradation of mechanical properties (mainly fatigue life), facilitated crack propagation, anisotropy, reduced corrosion resistance | Archimedes method, ultrasonic pulse-echo velocity measurements, image analysis of metallographic cross-sections, X-ray micro-computed tomography (μ -CT), hard X-rays in synchrotron facilities, gas pycnometry | Process optimization, control of the powder feedstock's composition and quality, HIP post-print treatment |
| Cracking and delamination | High cooling rates and thermal gradients, either too high or too low energy input, physical and metallurgical properties of the deposited material | Degradation of both static and dynamic mechanical properties, reduced corrosion resistance, premature failure | Metallographic cross-sections, crack opening and fractography in SEM; NDT: magnetic particles, radiography, μ -CT, ultrasonic, computational modeling | Process and geometric optimization, e.g., substrate and chamber preheating, materials compatibility when printing jointly multi-materials |
| High surface roughness | Low heat input, large powder particles, high laser scanning speeds; a variety of material feedstock, part design, processing, and post-processing conditions and variables | Adverse effects on dimensions and geometric tolerances, degradation of mechanical properties (particularly fatigue) | Contact or non-contact profilometry (including AFM and CLSM), SEM | Increase of heat input, small layer thickness, finer powder particles, post-processing (e.g., HIP and chemical/electrochemical polishing) |

in DED are similar to those in fusion welding [12]. Residual stresses are classified into three types based on the size of their effects, from macro-stresses (Type I) to atomic-scale stresses (Type III) [130].

Effects of residual stresses on deposited materials and parts: Residual stresses in AM parts might have a multitude of consequences, including residual stress-driven phase transformations [131], distortion [12,122,130], loss of geometric tolerance [12], cracking [29,132,133], delamination of parts from the substrate [132], early crack propagation under cyclic loading [12,130,134,135], and, as a result, premature failure of structural components.

Residual stress measurement: Residual stress measurement is a non-trivial task. Calculation of residual stresses requires the acquisition of some other measurable quantities, e.g., displacement/distortion, lattice spacing, or sound speed. Residual stress measurement techniques are typically classified into destructive and non-destructive. Destructive techniques are based on mechanical stress relaxation and include hole drilling [57,136–139], serial sectioning, and ring-core drilling. Non-destructive techniques are based on measuring lattice spacing (diffraction techniques) [137,140–143], speed of sound [136,137], or Barkhausen noise (sound emitted by a ferromagnetic material under an external magnetizing field) [136,144]. Most approaches are based on assumptions, and care needs to be taken to ensure these assumptions are valid for the specific component of interest. A detailed review of residual stress measurement techniques can

be found in [136–140]. Computational models, which are based on the numerical solution of thermal-stress equilibrium equations, are often also employed to describe the evolution of stresses and displacements as a function of time in 3D models [12].

Mitigation: One of the most popular residual stress reduction approaches is preheating of the substrate [12], building chamber, and the printed part during deposition. This allows a reduction of the overall thermal gradients in part during printing, minimizing the accumulated residual stresses. Corbin et al. [147] demonstrated that preheating the substrate to ~400 °C can reduce the substrate distortion accumulated during printing the first layer by 27.4%. Lu et al. [122] developed a 3D thermo-mechanical FEA to study distortions and residual stresses induced by DED. Their findings indicate that when substrate preheating is combined with build chamber heating, both the residual stresses and distortions can be reduced by up to 80.2% and 90.1%, respectively (Fig. 11e). Vasinonta et al. [146] also formulated a thermo-mechanical model to study temperature gradients and part and baseplate preheating on the residual stress of stainless steel parts fabricated by LENS. Their results suggest that uniform part and baseplate preheating considerably reduces the residual stress. The maximum reduction of ~40% residual stress was achieved by preheating the part and the baseplate to 400 °C (Fig. 11f). These studies show that preheating of the substrate, build chamber, and the printed parts provide a practical approach for residual stress mitigation; however, preheating does

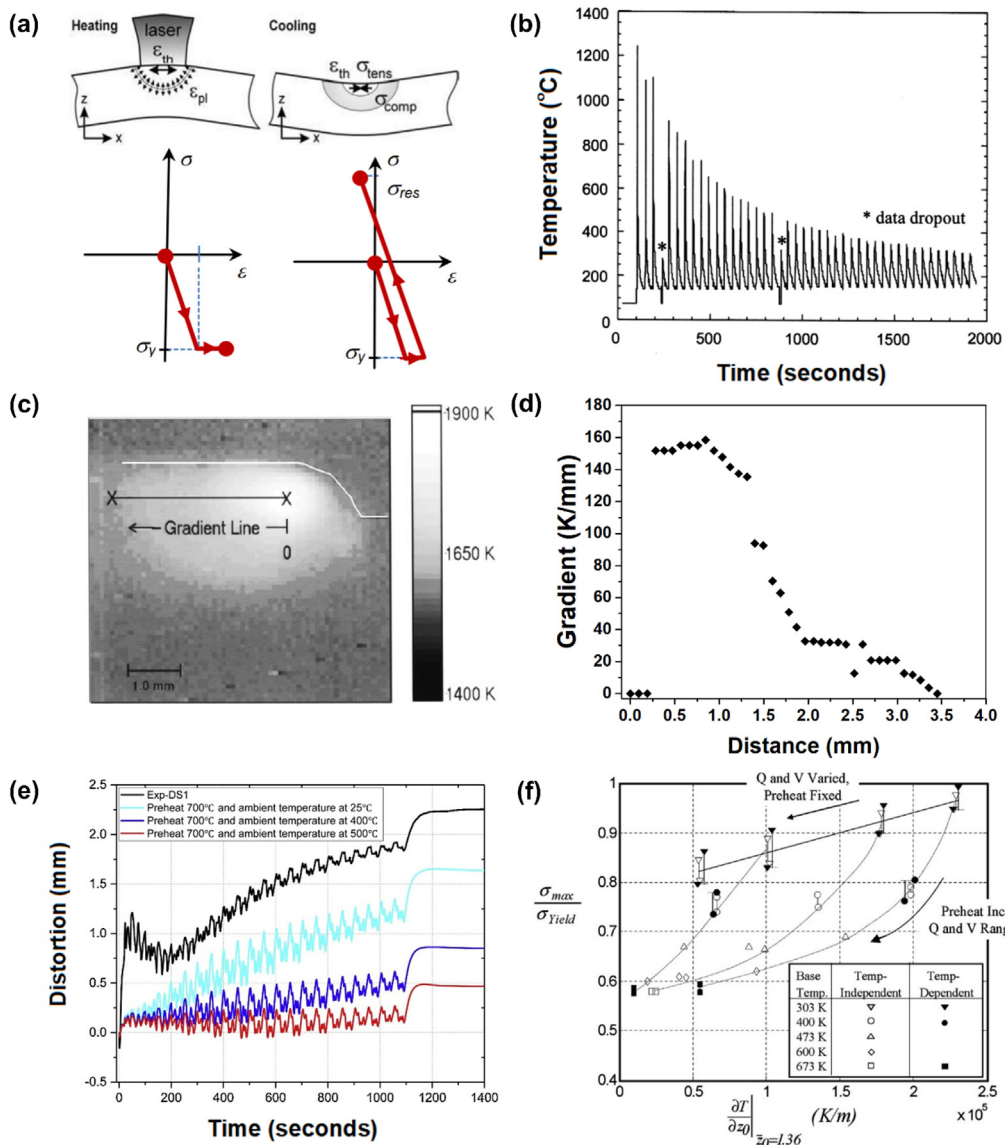


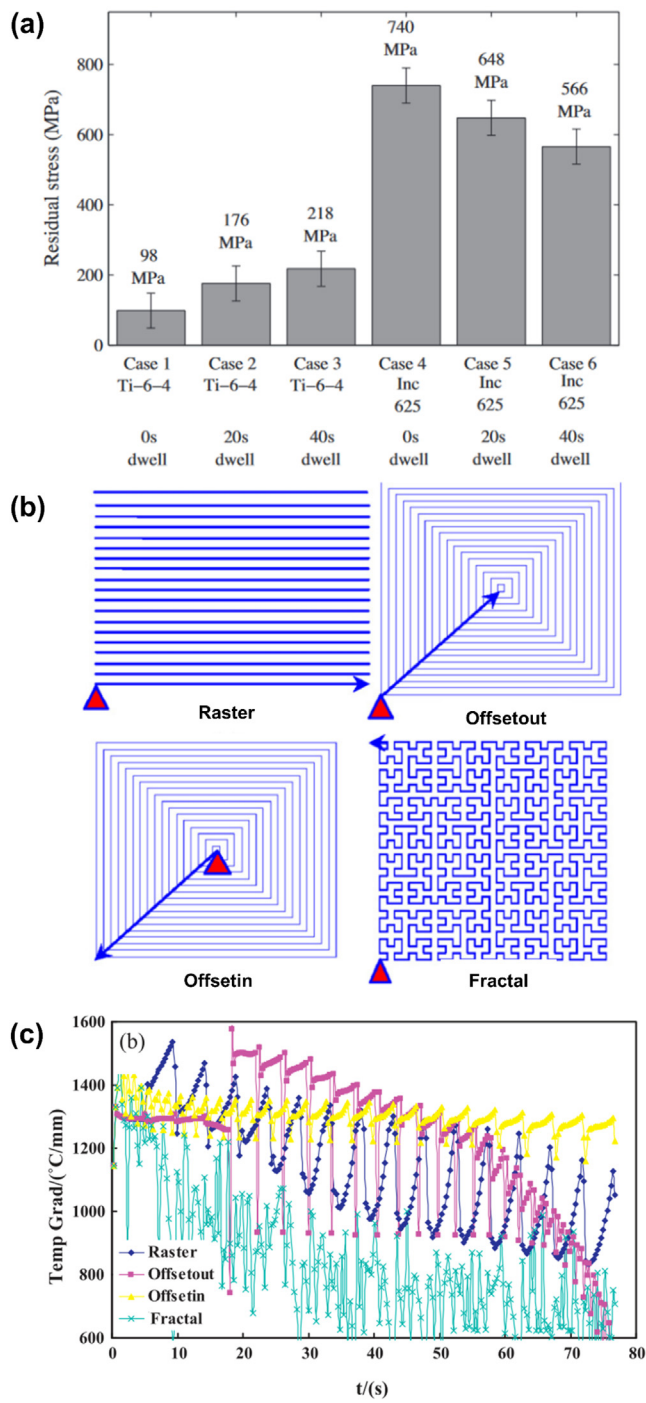
FIGURE 11

Origin of residual stresses in DED. (a) Model for residual stress formation: heating phase (left) and cooling phase (right). Reprinted from Ref. [145], with permission from Elsevier. (b) Response during LENS fabrication, demonstrating a complex thermal history of the printed part. Reprinted from Ref. [57], with permission from Elsevier. (c) Digital image of the molten pool during laser DED of 316 SS, and (d) temperature gradient along the gradient line, demonstrating large temperature gradients during DED. Reprinted from Ref. [57], with permission from Elsevier. *Influence of the preheating on the distortion and residual stress during DED:* (e) Calculated distortion generated during laser DED of Ti-6Al-4V. Preheating of the build chamber reduces the accumulated distortion. Reprinted from Ref. [122], with permission from Elsevier; (f) Influence of the part and baseplate preheating on thermal gradients and the resulting residual stress. Higher preheating temperatures lead to lower thermal gradients and, consequently, lower residual stresses. Reprinted from Ref. [146], with permission of the ASME.

not eliminate the residual stresses. Further post-processing might be required.

Another approach for residual stress mitigation during printing is optimizing the scan strategy [12,29]. Shorter deposition length, scanning in smaller islands, spiraling-in deposition strategy (as opposed to spiraling-out), increased scan speed, and decreased layer thickness to below the melt pool depth were all found beneficial for mitigation of both residual stresses and distortions [12,29]. The setting of track width and hatch spacing should make beads overlap [29]. Denlinger et al. [148] employed a series of *in situ* and post-process distortion measurements on Ti-

6Al-4V and Inconel 625 parts processed by laser DED to study the effect of interlayer dwell time on part distortion. They demonstrated that increasing the interlayer dwell time from zero to 40 s during deposition of Inconel 625 allows for additional cooling during deposition and reduces residual stress from ~710 MPa to ~566 MPa. On the other hand, the increase of dwell time from zero to 40 s during the printing of Ti-6Al-4V resulted in an increase of residual stress from ~98 MPa to ~218 MPa (Fig. 12a). These findings show that the development and evolution of residual stress are highly material-dependent. Specifically, differences in the behavior of Inconel 625 and Ti-6Al-4V may be

**FIGURE 12**

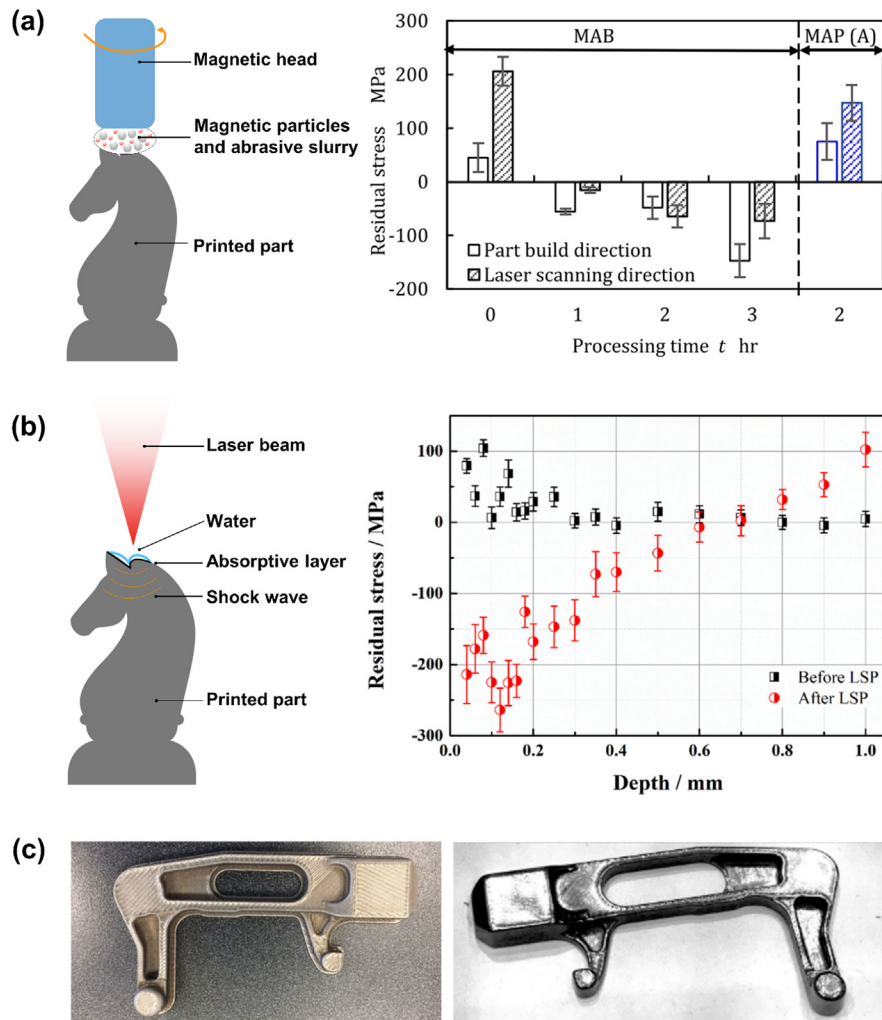
Residual stress mitigation by scan strategy optimization. (a) Influence of the interlayer dwell time on the residual stress in Inconel 625 and Ti-6Al-4V. Reprinted from Ref. [148], with permission from Elsevier. (b) Deposition patterns by LSF, and (c) FE modeling results showing the influence of scan strategy on the temperature gradients during laser DED. (b and c) Reprinted from Ref. [150], with permission from Elsevier. The lowest gradients are obtained with a fractal scan strategy following a Hilbert curve.

attributed to differences in phase transformations during printing. Woo et al. [149] investigated the influence of scan strategy on the residual stress in FGM prepared by laser DED. Results of the study show that the range of stress $\Delta\sigma$ can be reduced from

~950 MPa for 0° hatch rotation to ~680 MPa for 90° hatch rotation, and then further reduced to ~430 MPa for island or “checkerboard” strategy. Yu et al. [150] employed a fractal scanning strategy, where the layers were scanned following a Hilbert curve (Fig. 12b), namely a continuous fractal space-filling curve. They demonstrated that the parts printed with this strategy exhibited lower substrate deformations than conventional scan strategies due to the quasi-symmetric temperature distribution at the end of the deposition process and lower temperature gradients introduced by the fractal scanning strategy (Fig. 12c). These studies demonstrate that scan strategy has a large influence on the residual stresses and distortion in DED.

Residual stresses can be further decreased by post-print heat treatment. *In situ* compression tests were performed to study the stress relaxation induced by heat treatment of Inconel 625 parts via neutron diffraction [151]. The evolution of stresses within both additively manufactured and conventionally processed parts was quantified, and the analysis of both macroscopic stress and stress in grains with different crystallographic orientations was performed. At the same temperature and applied strain, AM-processed parts exhibited higher stress relaxation rates than those of the conventionally processed parts, regardless of the crystallographic orientation of the grains. Additionally, AM-processed parts demonstrated lower peak and plateau stresses as compared to conventionally processed parts. This difference was attributed to differences in texture and grain size of the two materials. Employing neutron diffraction, it was demonstrated [152] that residual stress in laser-DED-printed Inconel 625 parts can be relieved by heat treatment at 870 °C in Ar for 1 h. However, heat treatment also leads to precipitation of carbides, which reduces the reference strain-free lattice spacing, leading to potential errors in the computation of residual stresses. Zhang et al. [153] further analyzed the phase composition and precipitation kinetics of Inconel 625 at temperatures relevant to stress-relief heat treatments. Their findings indicate that elemental segregation caused by AM processing is the root cause for unusual precipitation behavior in heat-treated Inconel 625. These studies indicate that post-print heat treatment is an effective strategy for residual stress relief [29], but alloy-specific strategies must be developed to avoid the formation of undesirable phases.

Post-print surface treatments have been successfully employed to adjust the stress state of DED parts. For example, magnetic field-assisted finishing (MAF) was found to reduce residual stresses on AM parts' surface from ca. 200 MPa to ca. -70 MPa, converting the tensile stress into compressive on the part's surface [154], as shown in Fig. 13a. Residual stresses and distortion in WAAM parts can also be reduced by mechanical tensioning of the substrate or intermediate rolling of deposits [12]. Laser shock peening (LSP) has been explored as a post-print treatment to modify the surface stress in laser-DED Ti-6Al-4V parts [155]. This approach allowed for modification of residual surface stresses from ca. 100 MPa to ca. -200 MPa (Fig. 13b) and increased microhardness from ca. 361 VHN to ca. 420 VHN. LSP was also applied to WAAM 2319 aluminum alloy, introducing compressive stresses of up to -100 MPa [156]. Fig. 13c shows examples of chemically polished metal AM parts before and after finishing [157]. This particular part

**FIGURE 13**

Effect of post-print surface treatment on residual stress. (a) Magnetic field-assisted finishing modifies tensile surface residual stress into compressive residual stress. Reprinted from Ref. [154], with permission from Elsevier. (b) Laser shock peening converts tensile surface residual stress of ~100 MPa into compressive residual stress of ca. -200 MPa. Reprinted from Ref. [155], with permission from Elsevier. The cartoons illustrate the difference between the two surface treatment processes. (c) FormAlloy-produced door handle for the commercial aerospace industry with the as-printed surface (left) and the chemically-polished surface (right). Reprinted from [157], with permission from FormAlloy, CA.

was a quick built using FormAlloy's (San Diego, CA) laser-based DED set-up as a door handle for the aerospace industry. It can be seen that simple chemical polishing can improve the surface finish and reduce the layering marks in DED-processed metal AM parts. LSP also dramatically increased the surface microhardness of the WAAM parts, from ca. 75 VHN to ca. 110 VHN. These studies show that post-print surface modification can introduce surface compressive stresses, potentially improving DED-printed parts' fatigue life.

To conclude, DED is a non-equilibrium processing technique with characteristic high heating and cooling rates, high-temperature gradients, and complex thermal histories, which frequently leads to the development of residual stresses, porosity, and other defects. While considerable efforts have been made to measure, model, and alleviate residual stresses in AM parts, fundamental and holistic understanding of the mechanisms responsible for residual stress development remains a challenge.

Numerous studies show that optimizing process parameters and scan strategy can reduce residual stresses in as-printed parts; however, post-processing (e.g., hot isostatic pressing (HIP) or surface treatment) is still required to relieve residual stresses fully. This adds additional steps to the manufacturing process, increasing its total cost. Accurately measuring residual stresses in DED parts is also a challenge due to a tradeoff between time, cost, and accuracy in stress measurement techniques. This imposes additional limitations on residual stress studies, where typically only a few samples are measured, contributing to challenges in finding statistically significant differences. Lastly, most residual stress studies are performed on alloys common in AM, e.g., Inconel 625 and 718, 304 and 316 stainless steels, Ti-6Al-4V, and AlSi10Mg. Given that residual stress formation and evolution are material-specific, understanding these mechanisms in other materials, such as metal matrix composites and FGMS, must be developed.

Porosity

Origin of porosity: Porosity is one of DED's most common defects. It is typically formed via three main mechanisms [8,12,29,44,70,158–160]: (1) keyholes [161], which arise due to high energy density during deposition and causes localized vaporization and gas entrapment (Fig. 14a); (2) gas porosity originating from the feedstock, selective evaporation of an element in the alloy during melting, or entrapment of the shielding inert gas in the molten pool; and (3) lack of fusion (LoF) caused by insufficient penetration of the melt pool into the substrate or previously deposited layer, i.e., insufficient energy input (Fig. 14b). It is also common to distinguish between interlayer porosity (i.e., LoF) and intralayer porosity. The latter is typically distributed randomly through the bulk of the sample [163].

In terms of their shape, keyholes are relatively large pores that are either circular horizontally and elongated in the build direction or wider at the top than the bottom. Gas pores, on the other hand, are the smallest and most spherical of all pores. Finally, LoF pores are typically large (of a similar length scale to the melt pool size) and irregular in shape [164]. Sphericity factors may aid in distinguishing between different types of porosity [70,165,166]. Values lower than 0.6, higher than 0.7, and higher

than 0.92 have been related to LoF or partially melted powder particles, keyholes, and gas porosity, respectively [165,166].

Since porosity degrades the mechanical properties and facilitates crack nucleation and propagation, density measurement is one of the first, main quality control tests of deposited materials. In process optimization, the goal is often to achieve a density higher than 99.5% [8]. In powder DED, porosity depends on the powder feed rate (Fig. 14c) and energy input defined by laser power, laser spot size, and scan speed [8,23,158,162], as well as on powder porosity [159].

Effects of porosity on deposited materials and components: Porosity has a direct and adverse influence on both the mechanical properties, in particular the fatigue resistance [163,167–169], anisotropy [169], oxidation and corrosion resistance [170–174,176] of the printed parts. Since irregular or clustered pores could act as stress concentrators, they are considered more harmful to mechanical properties than spherical pores [8], particularly if they are oriented perpendicularly to the loading direction [174]. Due to the complex effect of pore geometry and location on the extent to which the fatigue life is reduced, the scatter in fatigue data might be high, and the uncertainty is increased [70]. The fatigue life of LENS-deposited Ti-6Al-4V was found to

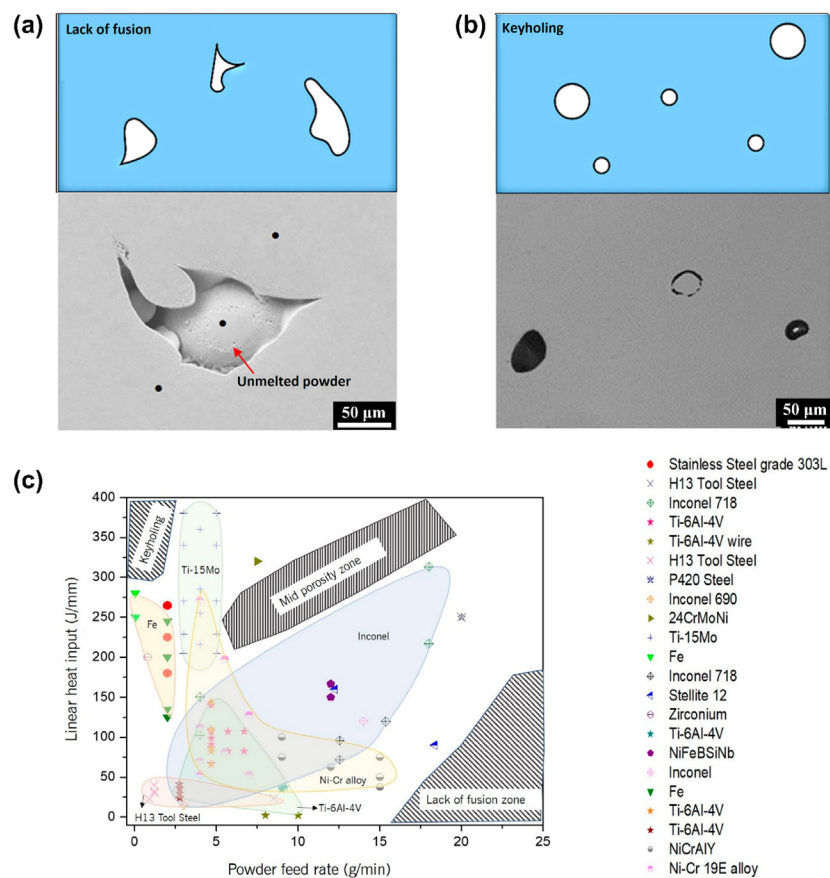


FIGURE 14

Origin and types of porosity in DED. (a) A schematic and an SEM micrograph of LOF porosity in 316L SS. Reprinted from Ref. [175]. Copyright 2009 by The Minerals, Metals & Materials Society. Used with permission. (b) A schematic and an SEM micrograph of keyholing porosity in Ti-6Al-4V. SEM images reprinted from Ref. [187], with permission from Elsevier. Top blue schematics are reproduction of Fig. 6a and b in Ref. [19], with permission from MDPI. (c) Relationship between the linear energy density, powder feed rate, and porosity for various metals and alloys. Reprinted from Ref. [19], with permission from MDPI.

be affected mainly by pore size (larger pores having a more detrimental effect), the number of pores – but only those close to the surface, and in the case of low cycle fatigue (LCF), pore shape, the distance between neighboring pores (densely-grouped pores are having a more pronounced effect) [168].

Porosity measurement: Recent efforts in process optimization and *in situ* process control have enabled routine DED fabrication of parts with >99% density [44,70,72,75,162,177–179]. Several methods for measuring the porosity/density of AM parts exist, including the Archimedes method [12,44,180–182], ultrasonic pulse-echo velocity measurements [44,180], image analysis of metallographic cross-sections [12,70,177,183,184], X-ray micro-computed tomography (μ -CT) [12,44,70,175,185,186], hard X-rays in synchrotron facilities [65,187], and gas pycnometry [180].

Mitigation: The most straightforward approach for porosity management in DED is process optimization. Process optimization involves adjusting parameters such as laser power, scan speed, hatch spacing, layer thickness, and powder feed rate. Combined parameters, such as linear energy density (LED, J/mm), areal energy density (AED, J/mm²), volumetric energy density (VED, J/mm³), and powder density (J/mm) are often employed in optimization [12,188]. Nevertheless, while there is a consensus that interlayer porosity (LoF) can be minimized through adjustment of process parameters, the origin of intra-layer porosity is less specific, hence it is often not straightforward to reduce it via process parameters [158,159]. Liu et al. [162] employed an analysis of variance (ANOVA) to study the influence of the process parameters in laser DED on the porosity of AlSi10Mg parts. They found that the most significant parameter is laser power, contributing ~49% to the relative density, followed by scan speed contributing ~34%. They demonstrated that low VED led to LoF porosity formation, while high VED led to keyholing and formation of spherical pores; a maximum density of >99% was achieved at 125 J/mm³. Dass and Moridi [19] compiled a process map with the optimized process parameters for DED of various materials (Fig. 14c), including Inconel, Ti-6Al-4V, H13 tool steel, Fe, Ti-15Mo, and some Ni-Cr alloys. They observed that the map contains three regions with no optimal data points, which could be attributed to keyholing, LoF, and mixed-mode porosity regimes dominating these regions.

Controlling the powder feedstock's composition and quality is also essential for porosity minimization in DED, as some of the gas porosity in the printed parts is introduced by powder feedstock. Ahsan et al. [158] compared porosity in parts fabricated from gas atomized (GA) and plasma rotating electrode (PREP) Ti-6Al-4V powders. They found the porosity in parts printed from PREP powder to be consistently lower than in parts printed from GA powder. The powder's chemical composition, including oxygen and moisture content, can also dramatically influence AM parts' porosity. Leung et al. [176] employed *in situ* and *operando* synchrotron X-ray imaging to examine powder oxidation's effects on porosity in Invar 36. They evaluated powders in the as-supplied condition (0.057 vol.% O) and after ~1 year of storage (0.343 vol.% O). Their results suggest that the powder feedstock's oxides acted as nucleation sites for pore formation, subsequently stabilizing the pores. Zhong et al. [189] demonstrated the effect of moisture and powder drying treatment on Inconel 718 deposits' porosity. They found that drying the powder at 110 °C for

~6 h led to a substantial porosity reduction, from ~0.41% to ~0.07%. These studies highlight the importance of feedstock powder control for porosity management in DED.

Porosity in DED parts can be closed with post-print treatment, such as HIP [163]. Qiu et al. [187] investigated HIP's influence on the microstructure and tensile properties of selective laser melting (SLM) Ti-6Al-4V parts. They found that HIP closed almost all of the samples' porosity, decreasing the pore area fraction from ~0.35% in the as-built condition to <0.01% in the HIPed condition. Kobryn et al. [169] also employed HIP to decrease porosity in Ti-6Al-4V LENS parts. The parts were HIPed for 2 h at 900 °C and 100 MPa, resulting in the closing of LoF porosity and, as a consequence, dramatically improved ductility. Despite the above, it has been argued that HIP is not a reliable process for removing entrapped gases from builds [163,190].

To conclude, most of the existing porosity studies are focused on investigating a particular metal or alloy and cannot be extended to the DED process in general. A more thorough understanding of how the material properties (e.g., laser absorptivity, coefficient of thermal expansion, thermal conductivity, and surface tension) affect the formation and evolution of porosity during DED is needed to reduce the time spent on process optimization.

Cracking and delamination

Origin of cracking and delamination: Delamination and cracking are most common in layered manufacturing in general, but in the case of DED and some other AM techniques, they are further enhanced by thermal stresses resulting from the cycles of rapid heating and cooling [132]. Delamination (namely, a separation between two consecutive layers or between the first deposited layers and the baseplate) results from the generation of interlayer residual stresses higher than the material's yield strength [12]. Delamination typically results from either incorporating unmelted/partially melted powder or insufficient remelting of layers underneath the melt pool [191]. It often occurs at the interface between the build and the baseplate, where high-stress concentrations exist.

Cracking in AM-fabricated parts plays a significant role in hindering widespread industrial adoption of metal AM [191,192]. It is highly dependent on the deposited material, namely, metals and alloys that are susceptible to cracking in fusion welding are likely to be susceptible to cracking during AM processing [192]. The major types of cracking in AM'ed parts are [12,191,192]: (i) Solidification cracking [193], also known as hot cracking, along grain boundaries. It is the consequence of the higher contraction of the top, hotter layers compared to the underlying layers or baseplate, resulting in the evolution of high tensile stresses [191,192]. This cracking might occur when the energy applied in the process is too high for the specific material, and it depends, among others, on the nature of solidification [191]; (ii) Liquation cracking [193] in the 'mushy', or partially melted zone (PMZ) of the build. It results from the melting of some grain-boundary precipitates during rapid heating to below the liquidus temperature and the evolution of tensile stresses in the partially melted zone due to both solidification and thermal contraction during cooling [12,191,192]. Alloys with a larger difference between the solidus and liquidus temperatures (e.g., Ni-

based superalloys), large solidification shrinkage (e.g., Ti–6Al–4V), and large thermal contraction (e.g., Al-based alloys) are most susceptible to this cracking [12]; and (iii) ductility dip cracking, a solid-state intergranular cracking encountered by some alloys with face-centered cubic (fcc) structure at elevated temperatures [192].

Effects of cracking and delamination on deposited materials and parts: Cracking and delamination result in degradation of both static and dynamic mechanical properties, decreased corrosion resistance, and premature failure.

Cracking characterization: Cracking and delamination can be characterized by both destructive and non-destructive tests, as well as by computational modeling. Destructive tests include metallographic cross-sections as well as opening of cracks and their characterization (fractography) by scanning electron microscopy (SEM). Non-destructive testing (NDT) includes, among others, magnetic particles, radiographic, μ -CT, or ultrasonic testing.

Mitigation: The only way to mitigate the problem of delamination and cracking is to prevent their formation. This can be done by process optimization, including substrate and chamber pre-heating, optimizing cooling rates, constraining aspect ratios and wall thicknesses, optimizing scan strategy and part orientation within the build, and assurance of materials compatibility when printing multi-materials together.

High surface roughness

Origin of surface roughness: DED is a near-net-shape process, implying that complementary post-processing, e.g., machining or polishing, is necessary to reach the required tolerances and surface quality. The high surface roughness of DED'ed parts may result mainly from: (i) Sticking to the surface of partially melted powder particles due to low heat input and large powder particles [12,194,195] and balling due to Raleigh instability at high laser scanning speeds that break the molten pool into small islands that are dragged to the outer edges of the molten pool [12,192]; (ii) Stair stepping effect, which limits all layered manufacturing processes, particularly when forming inclined or curved surfaces [196]; (iii) Splashing of molten material [197]. Surface roughness is determined by various material feedstock, part design, processing, and post-processing conditions and variables [12].

Effects of surface roughness on deposited materials and parts: Surface roughness affects the dimensions and geometric tolerances of the deposited parts and critically affect their mechanical properties, particularly fatigue. It has been reported that surface roughness of $\sim 200 \mu\text{m}$ can lower the fatigue strength by 20–25%, depending on the AM process [198].

Surface roughness measurement: Surface roughness can be measured by a variety of analytical techniques such as contact (e.g., atomic force microscopy (AFM) or stylus) or non-contact (e.g., confocal laser scanning microscopy (CLSM) or white light interferometry) profilometry and SEM. Recently [70], a novel, non-standard optical gaging procedure for measuring surface roughness of DED-processed alloys was suggested, employing a commercial video and a multisensory measurement system with large measurement range. The results compared well with those from white light interferometry.

Mitigation: Surface roughness can be reduced by increasing heat input (as long as it is not too high, introducing high thermal stresses and non-uniform solidification rate). This is achieved, for example, by high laser power and low scanning speed. Other approaches include the use of small layer thickness and finer powder particles. Finally, post-processing operations such as HIP and chemical/electrochemical polishing are often employed.

Defects in wire-fed DED-processed materials

The previous subsections already mentioned some defects-related aspects of wire-fed DED-processed materials. This section is aimed to add more details and provide a concise summary. Residual stresses, porosity, high surface roughness, and cracking are all relevant defects to WAAM-processed metal parts too. They are associated with both improper processing conditions (e.g., either insufficient or excessive energy input, spatter ejection, or poor path planning) and feedstock attributes (e.g., contamination of the wire or substrate) [199]. Porosity, mainly due to gas entrapment, is the most common defect in WAAM. Gap or void generation due to spattered ejection or insufficient melting is often observed in complex deposition paths or during a changeable manufacturing process. Besides, surface contamination of the wire and substrate, in the form of moisture, dirt, or grease, can absorb energy during deposition and form porosity after solidification [200]. Additionally, portions of unmelted wire might appear stuck to WAAM-processed parts [25]. The complex thermal cycles occurring during WAAM processing result in a mixed microstructure throughout the built, unfavorable for mechanical properties [201]. The surface roughness of wire-fed DED-processed parts might be high due to large molten pool sizes, bead widths, and layer thicknesses [12]. Like in powder-fed DED, residual stresses are generated in WAAM-fabricated parts [25]; they can be higher than the yield strength of the deposited metal, causing large distortion of the deposited part, poor tolerances, cracking, and delamination [25,199].

Residual stresses in WAAM can be significantly reduced by optimizing the deposition paths, substrate preheating, regulation of dwell time, post-processing heat treatment [25,201,202], or mounting the substrate on a 5-axis system and building parts on both sides so that the residual stresses are balanced [25]. A scan strategy starting from the edges to the center was found to cause fewer residual stresses on the substrate [25]. Lee et al. [203] reported a 50% reduction in residual stress by using a bidirectional tool path with 180° rotation, which can reduce crack formation potential at the bottom corner of the part. Cold rolling and ultrasonic impact testing were also found to reduce residual stresses in WAAM parts [25]. Side collapse and unmelted wire can be prevented by introducing sensors to guarantee a constant contact-tip-to-work distance and a constant interlayer temperature [25]. Bimetallic components show higher residual stress and subsequent deformations than single-metal components due to mismatch in the metals' thermal expansion.

Future directions

Because of DED's inherent flexibility and unique abilities, this technology's future is very exciting. Among key areas that we have discussed so far, perhaps the repair of parts using DED

has the most promising future. Although DED will not replace traditional welding stations, it will be significantly cheaper to repair high-value or one-of-a-kind parts than manufacturing them. Moreover, adding different alloys to increase the service life will make DED-based repair more exciting than just welding. The DED platform will be used to repair with similar alloys and deposit metal-ceramic composites during repair to increase service life or improve implants' biocompatibility [204,205]. It is also envisioned that DED will be popular in multi-material AM areas, including microstructural designs that can be naturally architected [13,47]. Multi-material structures can only be manufactured in one operation using DED or HAM platforms. The ability to tailor application-specific properties at different locations can be a disruptive technology in the coming years. To make it more viable, advances in multi-materials CAD and related FE analysis and topology optimization technologies need to mature further to offer reliability and reproducibility in those multi-material parts. Further improvements in slicing software such as adaptive and/or locally adaptive slicing and tool path generation software sensitive to different materials deposition in one build at different locations will make multi-materials AM more easily doable. Apart from metals and alloys, DED is also expected to impact direct ceramic processing for oxide and carbide-based ceramics or high-temperature boride or nitride-based ceramics [206,207]. The DED of ceramics can be of use for hard coatings or small size specialty bulk ceramic structures. And finally, it is expected that new alloys will be designed in the coming years using DED technology. The inherent flexibility in compositional modifications under a controlled environment and versatility in a large variety of metals and ceramics that can be processed via DED is a big plus in alloy design. Of course, complex part fabrication or addition of porous or dense coating on existing parts will also grow using DED as more and more users work with reliable machines and feel confident to use them in critical applications. The DED is a journey that will only be more attractive with time due to so many opportunities to explore, including applications that we can imagine today and others that we will only learn in the future.

Summary

We reviewed recent advances in directed energy deposition (DED) additive manufacturing (AM) technology, the associated processing science related to laser-material interactions, defects generation, and applications. Although currently less common than the powder bed fusion (PBF) technology for general metal AM applications, DED offers a lot more freedom in the materials domain, enabling fabrication of multi-material structures and alloy design. Moreover, DED is also becoming popular for large structures because of the build environment's freeform with 5-axis to free-axis deposition heads. Repair is another area of DED that is unique and has become popular for high-end metal parts. DED offers lower part resolution than PBF processes; however, when DED is used in a hybrid AM set-up, better dimensional tolerances can be achieved than in any other metal AM processes. Finally, in addition to powder feed, wire feed DED systems are also becoming popular, particularly for welding-based AM processes. Although the subject matter for DED AM is extensive, our article remained focused on recent advances in

fundamental processing science and related material applications along with current challenges and future directions. We envision that this article will help expand DED applications further, from structural to functional to biomedical devices in the coming years.

Declaration of Competing Interest

The authors declare that they have no known competing financial interests or personal relationships that could have appeared to influence the work reported in this paper.

Acknowledgments

DS and NE gratefully acknowledge the financial support from the Israel Ministry of Defense (grant no. 4440783376). ALV, BZ, JMS, and EJL wish to acknowledge financial support from the U. S. Army Research Office under grant W911NF-18-1-0279. AB and SB would like to acknowledge financial support from the US National Science Foundation under the grant number NSF-CMMI 1934230. BZ, JMS, and EJL are grateful for additional financial support from the Israel Ministry of Defense under P. O. No. 4440873734. We thank Mr. Kellen Traxel of Washington State University for his help with some of the figures.

References

- [1] J. Manyika, M. Chui, J. Bughin, R. Dobbs, P. Bisson, A. Marrs, *Disruptive Technologies: Advances that will Transform Life, Business, and the Global Economy*, McKinsey & Company, Washington DC, 2013.
- [2] G. Warwick, *Aviat. Week Space Technol.* 176 (11) (2014) 43–44.
- [3] M. Segrest, Print better parts, Efficient Plant, 17 September 2018, <https://www.efficientplantmag.com/2018/09/print-better-parts/> (accessed 14 December 2020).
- [4] Wohlers Report 2020: 3D Printing and Additive Manufacturing – State of the Industry, Wohlers Associates, Inc., Fort Collins, CO, 2020.
- [5] Ceramics Additive Manufacturing Markets 2017-2028, SmarTech Analysis, Crozet, VA, <https://www.smartechnalysis.com/reports/ceramics-additive-manufacturing-markets-2017-2028/> (accessed 14 December 2020).
- [6] ISO/ASTM 52900:2015(E): Standard terminology for additive manufacturing – general principles – terminology, ASTM International, West Conshohocken, PA, 2015.
- [7] A.G. Colomo et al., *Int. J. Rapid Manuf.* 9 (2020) 194–211, <https://doi.org/10.1504/IJRapidM.2020.107736>.
- [8] D. Herzog et al., *Acta Mater.* 117 (2016) 371–392, <https://doi.org/10.1016/j.actamat.2016.07.019>.
- [9] Metal additive manufacturing report, AMPOWER Report 2020, www.additive-manufacturing-report.com (accessed 27 January 2021).
- [10] SmarTech Analysis, Market opportunities for directed energy deposition manufacturing, <https://www.smartechnalysis.com/reports/market-opportunities-for-directed-energy-deposition-manufacturing/> (accessed 27 January 2021).
- [11] Optomec overview, <https://optomec.com/optomec-overview/> (accessed 14 December 2020).
- [12] T. DebRoy et al., *Prog. Mater Sci.* 92 (2018) 112–224, <https://doi.org/10.1016/j.pmatsci.2017.10.001>.
- [13] A. Bandyopadhyay, B. Heer, *Mater. Sci. Eng. R: Reports* 129 (2018) 1–16, <https://doi.org/10.1016/j.mser.2018.04.001>.
- [14] S. Liu, Y.C. Shin, *Mater. Des.* 164 (2019) 107552, <https://doi.org/10.1016/j.matdes.2018.107552>.
- [15] Y. Li et al., *Acta Biomater.* 77 (2018) 380–393, <https://doi.org/10.1016/j.actbio.2018.07.011>.
- [16] S.M. Yusuf, S. Cutler, N. Gao, *Metals* 9 (12) (2019) 1286, <https://doi.org/10.3390/met9121286>.
- [17] S.M. Thompson et al., *Addit. Manuf.* 8 (2015) 36–62, <https://doi.org/10.1016/j.adma.2015.07.001>.
- [18] N. Shamsaei et al., *Addit. Manuf.* 8 (2015) 12–35, <https://doi.org/10.1016/j.adma.2015.07.002>.
- [19] A. Dass, A. Moridi, *Coatings* 9 (7) (2019) 418, <https://doi.org/10.3390/coatings9070418>.

- [20] A. Saboori et al., *Appl. Sci.* 9 (16) (2019) 3316, <https://doi.org/10.3390/app9163316>.
- [21] J.M. Wilson et al., *J. Cleaner Prod.* 80 (2014) 170–178, <https://doi.org/10.1016/j.jclepro.2014.05.084>.
- [22] R.P. Mudge, N.R. Wald, *Weld. J.* 86 (2007) 44–48.
- [23] H. Wang et al., *Opt. Eng.* 59 (2020) 70901, <https://doi.org/10.11117/1.OE.59.7.070901>.
- [24] R.P. Martukanitz, Directed-energy deposition processes, in: D. Bourell, W. Frazier, H. Kuhn, M. Seifi (Eds.), *ASM Handbook*, Vol. 24: Additive Manufacturing Processes, ASM International, Materials Park, OH, 2020, pp. 220–238.
- [25] T.A. Rodrigues et al., *Materials* 12 (7) (2019) 1121, <https://doi.org/10.3390/ma12071121>.
- [26] S. Negi et al., *Rapid Prototyp. J.* 26 (3) (2019) 485–498, <https://doi.org/10.1108/RPJ-07-2019-0182>.
- [27] W.E. Frazier, *J. Mater. Eng. Perf.* 23 (6) (2014) 1917–1928, <https://doi.org/10.1007/s11665-014-0958-z>.
- [28] B. Wysocki et al., *Appl. Sci.* 7 (7) (2017) 657, <https://doi.org/10.3390/app7070657>.
- [29] I. Gibson, D. Rosen, B. Stucker, *Additive Manufacturing Technologies: 3D Printing, Rapid Prototyping, and Direct Digital Manufacturing*, 2nd ed., Springer, New York, NY, 2015, pp. 245–268. Ch. 10, https://doi.org.libproxy.mit.edu/10.1007/978-1-4939-2113-3_10.
- [30] ASTM F3187-16: Standard guide for directed energy deposition of metals, ASTM International, West Conshohocken, PA, 2016.
- [31] L. Nickels, *Met. Powder Rep.* 71 (2) (2016) 100–105, <https://doi.org/10.1016/j.mpr.2016.02.045>.
- [32] J. Gao, X. Chen, D. Zheng, Remanufacturing oriented adaptive repair system for worn components, in: 5th Int. Conf. Responsive Manufacturing – Green Manufacturing (ICRM 2010), Ningbo, China, 2010, pp. 13–18, <https://doi.org/10.1049/cp.2010.0406>.
- [33] T.D. Ngo et al., *Compos. B Eng.* 143 (2018) 172–196, <https://doi.org/10.1016/j.compositesb.2018.02.012>.
- [34] S.W. Williams et al., *Mater. Sci. Technol.* 32 (7) (2016) 641–647, <https://doi.org/10.1179/1743284715Y.0000000073>.
- [35] ASTM F3413-2019: Guide for additive manufacturing – design – directed energy deposition, ASTM International, West Conshohocken, PA, 2019.
- [36] V.T. Le, H. Paris, G. Mandil, J. *Manuf. Syst.* 44 (1) (2017) 243–254, <https://doi.org/10.1016/j.jmsy.2017.06.003>.
- [37] B. Zheng et al., *Mater. Sci. Eng., A* 764 (2019) 138243, <https://doi.org/10.1016/j.msea.2019.138243>.
- [38] LENS directed energy deposition (DED) 3D printed metal technology, <https://optomec.com/3d-printed-metals/lens-technology/> (accessed 28 January 2021).
- [39] P. Gradi, *Principles of Directed Energy Deposition for Aerospace Applications*, NASA Marshall Space Flight Center, 20 January 2021. <https://doi.org/10.13140/RG.2.2.10504.75527>.
- [40] B. Onuike, A. Bandyopadhyay, *Mater. Lett.* 252 (2019) 256–259, <https://doi.org/10.1016/j.matlet.2019.05.114>.
- [41] V.K. Balla et al., *Acta Biomater.* 6 (6) (2010) 2329–2334, <https://doi.org/10.1016/j.actbio.2009.11.021>.
- [42] M. Roy et al., *Acta Biomater.* 4 (2) (2008) 324–333, <https://doi.org/10.1016/j.actbio.2007.09.008>.
- [43] K.D. Traxel, A. Bandyopadhyay, *Addit. Manuf.* 37 (2021) 101602, <https://doi.org/10.1016/j.addma.2020.101602>.
- [44] D. Svetlikzky et al., *Mater. Des.* 192 (2020) 108763, <https://doi.org/10.1016/j.matdes.2020.108763>.
- [45] K. Knoll et al., *Steel Res. Int.* 88 (8) (2017) 1600416, <https://doi.org/10.1002/srin.201600416>.
- [46] Optomec advances aluminum directed energy deposition (DED) additive manufacturing, <https://3dprintingindustry.com/news/optomec-advances-aluminum-directed-energy-deposition-ded-additive-manufacturing-171579/> (accessed 28 January 2021).
- [47] K.D. Traxel, A. Bandyopadhyay, *Addit. Manuf.* 34 (2020) 101243, <https://doi.org/10.1016/j.addma.2020.101243>.
- [48] B. Onuike, B. Heer, A. Bandyopadhyay, *Addit. Manuf.* 21 (2018) 133–140, <https://doi.org/10.1016/j.addma.2018.02.007>.
- [49] B. Heer, A. Bandyopadhyay, *Mater. Lett.* 216 (2018) 16–19, <https://doi.org/10.1016/j.matlet.2017.12.129>.
- [50] B. Zheng, Y. Xiong, J. Nguyen, J.E. Smugeresky, Y. Zhou, E.J. Lavernia, J.M. Schoenung, Powder additive processing with laser engineered net shaping (LENS), in: L.J. Smit, J.H. van Dijk (Eds.), *Powder Metallurgy Research Trends*, Nova Science Publishers, Hauppauge, NY, 2009, pp. 125–190.
- [51] J.C. Haley et al., *Mater. Des.* 161 (2019) 86–94, <https://doi.org/10.1016/j.matdes.2018.11.021>.
- [52] J.I. Arrizubieta et al., *Int. J. Heat Mass Transf.* 115 (2017) 80–91, <https://doi.org/10.1016/j.ijheatmasstransfer.2017.07.011>.
- [53] V. Manvatkar, A. De, T. DebRoy, *J. Appl. Phys.* 116 (12) (2014) 124905, <https://doi.org/10.1063/1.4896751>.
- [54] A.J. Pinkerton, L. Li, *Proc. Inst. Mech. Eng. Part B J. Eng. Manuf.* 218 (2004) 363–374, <https://doi.org/10.1243/095440504323055498>.
- [55] A.J. Pinkerton, *J. Phys. D Appl. Phys.* 40 (23) (2007) 7323–7334, <https://doi.org/10.1088/0022-3727/40/23/012>.
- [56] Y. Xiong et al., *Acta Mater.* 57 (18) (2009) 5419–5429, <https://doi.org/10.1016/j.actamat.2009.07.038>.
- [57] M.L. Griffith et al., *Mater. Des.* 20 (2–3) (1999) 107–113, [https://doi.org/10.1016/S0261-3069\(99\)00016-3](https://doi.org/10.1016/S0261-3069(99)00016-3).
- [58] M.L. Griffith, M.T. Ensz, J.D. Puskar, C.V. Robino, J.A. Brooks, J.A. Philliber, J.E. Smugeresky, W.H. Hofmeister, Understanding the microstructure and properties of components fabricated by laser engineered net shaping (LENS®), in: *MRS Proc. Vol. 625*, 2000, <https://doi.org/10.1557/PROC-625-9>.
- [59] W. Hofmeister et al., *JOM* 53 (2001) 30–34, <https://doi.org/10.1007/s11837-001-0066-z>.
- [60] W. Wei, Y. Zhou, R. Ye, D. Lee, J.E. Craig, J.E. Smugeresky, E. Lavernia, Investigation of the thermal behavior during the LENS™ process, in: *Proc. Int. Conf. Metal Powder Deposition for Rapid Manufacturing*, San Antonio, TX, 2002, pp. 128–135.
- [61] W. Hofmeister, et al., *JOM-e* 51(7) (1999) <http://www.tms.org/pubs/journals/JOM/9907/Hofmeister/Hofmeister-9907.html>.
- [62] J.C. Haley, J.M. Schoenung, E.J. Lavernia, *Addit. Manuf.* 22 (2018) 368–374, <https://doi.org/10.1016/j.addma.2018.04.028>.
- [63] J.C. Haley, J.M. Schoenung, E.J. Lavernia, *Mater. Sci. Eng., A* 761 (2019) 138052, <https://doi.org/10.1016/j.msea.2019.138052>.
- [64] R. Cunningham et al., *Science* 363 (6429) (2019) 849–852, <https://doi.org/10.1126/science:aav4687>.
- [65] S.J. Wolff et al., *Sci. Rep.* 9 (1) (2019) 962, <https://doi.org/10.1038/s41598-018-36678-5>.
- [66] A. Heralić, A.K. Christiansson, B. Lennartsson, *Opt. Lasers Eng.* 50 (9) (2012) 1230–1241, <https://doi.org/10.1016/j.optlaseng.2012.03.016>.
- [67] A.I. Adediran, A. Nycz, A. Thornton, Visual sensing and image processing for error detection in laser metal wire deposition, in: *Proc. 28th Annu. Int. Solid Freeform Fabrication Symp.*, Austin, TX, 2017, pp. 2036–2044.
- [68] A. Heralić et al., *IFAC Proc. Vol.* 41 (2) (2008) 14785–14791, <https://doi.org/10.3182/20080706-5-KR-1001.02503>.
- [69] J. Edgar, S. Tint, *Johnson Matthey Technol. Rev.* 59 (3) (2015) 193–198, <https://doi.org/10.1595/205651315x688406>.
- [70] N. Eliaz et al., *Materials* 13 (18) (2020) 4171, <https://doi.org/10.3390/ma13184171>.
- [71] E.O. Olakanmi, R.F. Cochrane, K.W. Dalgarno, *Prog. Mater Sci.* 74 (2015) 401–477, <https://doi.org/10.1016/j.pmatsci.2015.03.002>.
- [72] J.B. Ferguson et al., *J. Manuf. Processes* 19 (2015) 163–170, <https://doi.org/10.1016/j.jmapro.2015.06.026>.
- [73] H.-J. Jiang, H.L. Dai, *Int. J. Heat Mass Transf.* 82 (2015) 98–108, <https://doi.org/10.1016/j.ijheatmasstransfer.2014.11.003>.
- [74] J.C. Heigel, P. Michaleris, E.W. Reutzel, *Addit. Manuf.* 5 (2015) 9–19, <https://doi.org/10.1016/j.addma.2014.10.003>.
- [75] M. Khanzadeh et al., *IIE Trans.* 51 (5) (2019) 437–455, <https://doi.org/10.1080/24725854.2017.1417656>.
- [76] Z.-J. Tang et al., *Int. J. Adv. Manuf. Technol.* 108 (2020) 3437–3463, <https://doi.org/10.1007/s00170-020-05569-3>.
- [77] D. Weisz-Patrault, *Addit. Manuf.* 31 (2020), <https://doi.org/10.1016/j.addma.2019.100990>.
- [78] X. Li et al., *Procedia Manuf.* 48 (2020) 643–649, <https://doi.org/10.1016/j.promfg.2020.05.093>.
- [79] A. Bandyopadhyay, K.D. Traxel, *Addit. Manuf.* 22 (2018) 758–774, <https://doi.org/10.1016/j.addma.2018.06.024>.
- [80] J. Ertveldt, P. Guillaume, J. Helsen, *Procedia CIRP* 94 (2020) 456–461, <https://doi.org/10.1016/j.procir.2020.09.164>.
- [81] Z. Zhu et al., *Procedia CIRP* 91 (2020) 534–539, <https://doi.org/10.1016/j.procir.2020.03.108>.
- [82] D.R. Feenstra, A. Molotnikov, N. Birbilis, *Mater. Des.* 198 (2021), <https://doi.org/10.1016/j.matdes.2020.109342>.
- [83] G. Wang et al., *Int. J. Refract. Metal Hard Mater.* 82 (2019) 227–233, <https://doi.org/10.1016/j.ijrmhm.2019.04.016>.
- [84] C. Zhong et al., *J. Laser Appl.* 27 (4) (2015) 042003, <https://doi.org/10.2351/1.4923335>.

- [85] K. Shah et al., Mater. Manuf. Processes 25 (12) (2010) 1372–1380, <https://doi.org/10.1080/10426914.2010.480999>.
- [86] N.A. Kistler et al., J. Laser Appl. 29 (2) (2017), <https://doi.org/10.2351/1.4979702>.
- [87] Y. Yao et al., Opt. Laser Technol. 105 (2018) 171–179, <https://doi.org/10.1016/j.optlastec.2018.03.011>.
- [88] M. Das et al., Trans. Indian Ceram. Soc. 72 (3) (2013) 169–174, <https://doi.org/10.1080/0371750X.2013.851619>.
- [89] Q. Chao et al., Surf. Coat. Technol. 332 (2017) 440–451, <https://doi.org/10.1016/j.surfcoat.2017.09.072>.
- [90] K. Zhang et al., Mater. Des. 55 (2014) 104–119, <https://doi.org/10.1016/j.matdes.2013.09.006>.
- [91] A. Reichardt et al., Mater. Des. 104 (2016) 404–413, <https://doi.org/10.1016/j.matdes.2016.05.016>.
- [92] J.L. Bennett et al., J. Manuf. Processes 28 (2017) 550–557, <https://doi.org/10.1016/j.jmapro.2017.04.024>.
- [93] T. Durejko et al., Mater. Sci. Eng., A 650 (2016) 374–381, <https://doi.org/10.1016/j.msea.2015.10.076>.
- [94] Y. Han et al., Mater. Res. 18 (Suppl. 1) (2015) 24–28, <https://doi.org/10.1590/1516-1439.322214>.
- [95] M. Shukla et al., Proc. World Acad. Sci. Eng. Technol. 6 (11) (2012) 2475–2479.
- [96] A.J. Pinkerton, J. Laser Appl. 27 (S1) (2015) S15001, <https://doi.org/10.2351/1.4815992>.
- [97] S. Sreekanth, Laser-directed energy deposition: Influence of process parameters and heat-treatments, Licentiate Thesis, Production Technology No. 30, University West, Trollhättan, Sweden, 2020, ISBN 978-91-88847-66-9.
- [98] R. Sampson et al., Opt. Laser Technol. 134 (2021) 106609, <https://doi.org/10.1016/j.optlastec.2020.106609>.
- [99] B. Bax et al., Addit. Manuf. 21 (2018) 487–494, <https://doi.org/10.1016/j.addma.2018.04.002>.
- [100] F.M. Sciammarella, B. Salehi Najafabadi, J. Manuf. Mater. Process. 2 (3) (2018) 61, <https://doi.org/10.3390/jmmp2030061>.
- [101] E. Toyserkani, A. Khajepour, S.F. Corbin, Laser Cladding, CRC Press, Boca Raton, FL, 2005.
- [102] K.D. Traxel et al., Manuf. Lett. 25 (2020) 88–92, <https://doi.org/10.1016/j.mfglet.2020.08.005>.
- [103] A. Simchi, H. Pohl, Mater. Sci. Eng., A 359 (1-2) (2003) 119–128, [https://doi.org/10.1016/S0921-5093\(03\)00341-1](https://doi.org/10.1016/S0921-5093(03)00341-1).
- [104] Z. Liu et al., J. Manuf. Process. 42 (2019) 96–105, <https://doi.org/10.1016/j.jmapro.2019.04.020>.
- [105] D.S. Shim et al., Opt. Laser Technol. 86 (2016) 69–78, <https://doi.org/10.1016/j.optlastec.2016.07.001>.
- [106] T. Kuriya et al., Seimitsu Kogaku Kaishi/Journal Japan Soc. Precis. Eng. 84 (4) (2018) 371–377, <https://doi.org/10.2493/jjspe.84.371>.
- [107] H.A. Macleod, Thin-Film Optical Filters, CRC Press, Boca Raton, FL, 2017.
- [108] J. Zhang et al., J. Mater. Sci. Technol. 35 (2) (2019) 270–284, <https://doi.org/10.1016/j.jmst.2018.09.004>.
- [109] I. Polmear, D. StJohn, J.-F. Nie, M. Qian, Light Alloys: Metallurgy of the Metals, 5th ed., Butterworth-Heinemann, Oxford, UK, 2017. <https://doi.org/10.1016/B978-0-08-099431-4.00010-5>.
- [110] M. Bauccio (Ed.), ASM Metals Reference Book, 3rd ed., ASM International, Materials Park, OH, 1993.
- [111] M. Boivineau et al., Int. J. Thermophys. 27 (2) (2006) 507–529, <https://doi.org/10.1007/PL000021868>.
- [112] M. Fujishima et al., CIRP J. Manuf. Sci. Technol. 19 (2017) 200–204, <https://doi.org/10.1016/j.cirpj.2017.04.003>.
- [113] V. Manvatkar, A. De, T. DebRoy, Mater. Sci. Technol. 31 (8) (2015) 924–930, <https://doi.org/10.1179/1743284714Y.0000000701>.
- [114] Y. Wang, J. Shi, Procedia Manuf. 26 (2018) 941–951, <https://doi.org/10.1016/j.promfg.2018.07.121>.
- [115] W. Yuan et al., Mater. Des. 189 (2020) 108542, <https://doi.org/10.1016/j.matdes.2020.108542>.
- [116] Y. Zhou et al., Mater. Sci. Eng. A 742 (2019) 150–161, <https://doi.org/10.1016/j.msea.2018.10.092>.
- [117] H.S. Prasad et al., J. Laser Appl. 31 (2019), <https://doi.org/10.2351/1.5096130>.
- [118] J. Lin, Opt. Laser Technol. 31 (3) (1999) 233–238, [https://doi.org/10.1016/S0030-3929\(99\)00046-8](https://doi.org/10.1016/S0030-3929(99)00046-8).
- [119] C. Zhong et al., Metals 7 (10) (2017) 443, <https://doi.org/10.3390/met7100443>.
- [120] Y.S. Lee et al., Welding J. 93 (2014) 292s–300s.
- [121] J. Lu, Prestress engineering of structural material: a global design approach to the residual stress problem, in: G. Totten, M. Howes, T. Inoue (Eds.), Handbook of Residual Stress and Deformation of Steel, ASM International, 2002, pp. 11–26.
- [122] X. Lu et al., Addit. Manuf. 26 (2018) 166–179, <https://doi.org/10.1016/j.addma.2019.02.001>.
- [123] K.L. Terrassa et al., Mater. Sci. Eng., A 765 (2019) 138269, <https://doi.org/10.1016/j.msea.2019.138269>.
- [124] F. Lia et al., Mater. Sci. Eng., A 717 (2018) 1–10, <https://doi.org/10.1016/j.msea.2018.01.060>.
- [125] B. Zheng et al., Metall. Mater. Trans. A 39 (9) (2008) 2228–2236, <https://doi.org/10.1007/s11661-008-9557-7>.
- [126] C. Kenel et al., Sci. Rep. 7 (1) (2017) 16358, <https://doi.org/10.1038/s41598-017-16760-0>.
- [127] D.A. Kriczky et al., J. Mater. Process. Technol. 221 (2015) 172–186, <https://doi.org/10.1016/j.jmatprotec.2015.02.021>.
- [128] B.A. Szost et al., Mater. Des. 89 (2016) 559–567, <https://doi.org/10.1016/j.matdes.2015.09.115>.
- [129] M. Strantza et al., Acta Mater. 168 (2019) 299–308, <https://doi.org/10.1016/j.actamat.2019.01.050>.
- [130] K. Carpenter, A. Tabei, Materials 13 (2020) 255, <https://doi.org/10.3390/ma13020255>.
- [131] T. LeBrun et al., Mater. Des. 81 (2015) 44–53, <https://doi.org/10.1016/j.matdes.2015.05.026>.
- [132] M. Alimardani et al., Opt. Lasers Eng. 47 (11) (2009) 1160–1168, <https://doi.org/10.1016/j.optlaseng.2009.06.010>.
- [133] D. Gu, B. He, Comput. Mater. Sci. 117 (2016) 221–232, <https://doi.org/10.1016/j.commatsci.2016.01.044>.
- [134] R. Chattopadhyay, Life-cycle assessment, in: G. Tribology (Ed.), Green Surface Engineering, and Global Warming, ASM International, Materials Park, OH, 2014, pp. 193–237.
- [135] J. Zhang et al., Mater. Des. 90 (2016) 551–561, <https://doi.org/10.1016/j.matdes.2015.10.141>.
- [136] N.S. Rossini et al., Mater. Des. 35 (2012) 572–588, <https://doi.org/10.1016/j.matdes.2011.08.022>.
- [137] P.J. Withers, H.K.D.H. Bhadeshia, Mater. Sci. Technol. 17 (4) (2001) 355–365, <https://doi.org/10.1179/02670830110150980>.
- [138] C.O. Ruud, NDT Int. 15 (1) (1982) 15–23, [https://doi.org/10.1016/0308-9126\(82\)90083-9](https://doi.org/10.1016/0308-9126(82)90083-9).
- [139] C. Ruud, Measurement of residual stresses, in: G. Totten, M. Howes, T. Inoue (Eds.), Handbook of Residual Stress and Deformation of Steel, ASM International, Materials Park, OH, 2002, pp. 99–117.
- [140] P.S. Prevey, X-ray diffraction residual stress techniques, in: ASM Handbook, Vol. 10: Materials Characterizations, ASM International, Materials Park, OH, 1986, pp. 380–392.
- [141] M.T. Hutchings, P.J. Withers, T.M. Holden, T. Lorentzen, *Introduction to the Characterization of Residual Stress by Neutron Diffraction*, Taylor & Francis, Boca Raton, FL, 2005.
- [142] W. Wu et al., Appl. Phys. Lett. 112 (25) (2018) 253501, <https://doi.org/10.1063/1.5026066>.
- [143] R. Pokharel et al., Int. J. Plast. 121 (2019) 201–217, <https://doi.org/10.1016/j.ijplas.2019.06.005>.
- [144] J. Gauthier, T.W. Krause, D.L. Atherton, NDT E Int. 31 (1) (1998) 23–31, [https://doi.org/10.1016/S0963-8695\(97\)00023-6](https://doi.org/10.1016/S0963-8695(97)00023-6).
- [145] C. Li et al., Procedia CIRP 71 (2018) 348–353, <https://doi.org/10.1016/j.procir.2018.05.039>.
- [146] A. Vasinonta, J.L. Beuth, M. Griffith, J. Manuf. Sci. Eng. Trans. ASME 129 (1) (2007) 101–109, <https://doi.org/10.1115/1.2335852>.
- [147] D.J. Corbin et al., J. Manuf. Sci. Eng. Trans. ASME 140 (6) (2018) 1–9, <https://doi.org/10.1115/1.4038890>.
- [148] E.R. Denlinger et al., J. Mater. Process. Technol. 215 (2015) 123–131, <https://doi.org/10.1016/j.jmatprotec.2014.07.030>.
- [149] W. Woo et al., Mater. Sci. Eng., A 744 (2019) 618–629, <https://doi.org/10.1016/j.msea.2018.12.078>.
- [150] J. Yu et al., Mater. Sci. Eng., A 528 (3) (2011) 1094–1104, <https://doi.org/10.1016/j.msea.2010.09.078>.
- [151] Z. Wang et al., Mater. Sci. Eng., A 714 (2018) 75–83, <https://doi.org/10.1016/j.msea.2017.12.058>.
- [152] Z. Wang et al., Mater. Des. 113 (2017) 169–177, <https://doi.org/10.1016/j.matdes.2016.10.003>.
- [153] F. Zhang et al., Acta Mater. 152 (2018) 200–214, <https://doi.org/10.1016/j.actamat.2018.03.017>.
- [154] H. Yamaguchi, O. Fergani, P.Y. Wu, CIRP Ann. 66 (1) (2017) 305–308, <https://doi.org/10.1016/j.cirp.2017.04.084>.

- [155] W. Guo et al., *Surf. Coat. Technol.* 349 (2018) 503–510, <https://doi.org/10.1016/j.surfcoat.2018.06.020>.
- [156] R. Sun et al., *J. Alloy. Compd.* 747 (2018) 255–265, <https://doi.org/10.1016/j.jallcom.2018.02.353>.
- [157] From aerospace engineering to AM: Melanie Lang on FormAlloy and the future of Directed Energy Deposition (DED), *Metal AM* 6(3) (2020) 145–152.
- [158] M.N. Ahsan, R. Bradley, A.J. Pinkerton, *J. Laser Appl.* 23 (2) (2011) 022009, <https://doi.org/10.2351/1.3582311>.
- [159] D.F. Susan et al., *Mater. Charact.* 57 (1) (2006) 36–43, <https://doi.org/10.1016/j.matchar.2005.12.005>.
- [160] F.H. Kim, S.P. Moylan, *NIST Adv. Manuf. Series* 100–16 (May 2018), <https://doi.org/10.6028/NIST.AMS.100-16>.
- [161] C. Zhao et al., *Science* 370 (6520) (2020) 1080–1086, <https://doi.org/10.1126/science:abbd1587>.
- [162] Y. Liu et al., *Opt. Laser Technol.* 111 (2019) 470–480, <https://doi.org/10.1016/j.optlastec.2018.10.030>.
- [163] A.W. Prabhu et al., *Sci. Technol. Weld. Join.* 20 (2015) 659–669, <https://doi.org/10.1179/1362171815Y.0000000050>.
- [164] D. Nursyifa Faulkhair et al., *J. Welding Join.* 37 (2019) 579–584, <https://doi.org/10.5781/JWJ.2019.37.6.7>.
- [165] R. Snell et al., *JOM* 72 (1) (2020) 101–109, <https://doi.org/10.1007/s11837-019-03761-9>.
- [166] J.C. Hastie et al., *Mater. Charact.* 163 (2020) 110225, <https://doi.org/10.1016/j.matchar.2020.110225>.
- [167] S.J. Wolff et al., *Acta Mater.* 132 (2017) 106–117, <https://doi.org/10.1016/j.actamat.2017.04.027>.
- [168] A.J. Sterling et al., *Mater. Sci. Eng., A* 655 (2016) 100–112, <https://doi.org/10.1016/j.msea.2015.12.026>.
- [169] P.A. Kobryn, S.L. Semiatin, **Mechanical properties of laser-deposited Ti-6Al-4V, AFRL/MLLMP, Wright-Patterson Air Force Base, OH, 2001**, pp. 179–186. <http://dx.doi.org/10.26153/tsw/3261>.
- [170] S.B. Hong et al., *Corros. Sci.* 43 (2001) 1781–1791, [https://doi.org/10.1016/S0010-938X\(00\)00181-5](https://doi.org/10.1016/S0010-938X(00)00181-5).
- [171] S.-B. Hong et al., *J. Dent. Res.* 80 (3) (2001) 860–863, <https://doi.org/10.1177/00220345010800030301>.
- [172] N. Eliaz, *Materials* 12 (2019) 407, <https://doi.org/10.3390/ma12030407>.
- [173] M.A. Melia et al., *Corros. Sci.* 152 (2019) 20–30, <https://doi.org/10.1016/j.corsci.2019.02.029>.
- [174] G. Kasperovich et al., *Mater. Des.* 105 (2016) 160–170, <https://doi.org/10.1016/j.matdes.2016.05.070>.
- [175] L. Wang, P. Pratt, S. Felicelli, H. Kadiri, P. Wang, Experimental analysis of porosity in laser-assisted powder deposition process, *Sppl. Proc. Vol. 1: Fabrication, Materials, Processing and Properties, TMS, 2009*, pp. 389–396.
- [176] C.L.A. Leung et al., *Acta Mater.* 166 (2019) 294–305, <https://doi.org/10.1016/j.actamat.2018.12.027>.
- [177] Z.E. Tan et al., *Addit. Manuf.* 25 (2019) 286–296, <https://doi.org/10.1016/j.addma.2018.11.014>.
- [178] M. Khanzadeh et al., *J. Manuf. Syst.* 47 (2018) 69–82, <https://doi.org/10.1016/j.jmsy.2018.04.001>.
- [179] P.A. Kobryn, E.H. Moore, S.L. Semiatin, *Scr. Mater.* 43 (4) (2000) 299–305, [https://doi.org/10.1016/S1359-6462\(00\)00408-5](https://doi.org/10.1016/S1359-6462(00)00408-5).
- [180] J.A. Slotwinski, E.J. Garboczi, K.M. Hebenstreit, *J. Res. Natl. Inst. Stand. Technol.* 119 (2014) 494–528, <https://doi.org/10.6028/jres.119.019>.
- [181] A.B. Spierings, M. Schneider, R. Eggenberger, *Rapid Prototyp. J.* 17 (5) (2011) 380–386, <https://doi.org/10.1108/13552541111156504>.
- [182] W.W. Wits et al., *CIRP Ann.* 65 (1) (2016) 201–204, <https://doi.org/10.1016/j.cirp.2016.04.054>.
- [183] J. Choi, Y. Chang, *Int. J. Mach. Tools Manuf.* 45 (4–5) (2005) 597–607, <https://doi.org/10.1016/j.ijmachtools.2004.08.014>.
- [184] W. Tillmann et al., *Addit. Manuf.* 13 (2017) 93–102, <https://doi.org/10.1016/j.addma.2016.11.006>.
- [185] X. Cai et al., *Virtual Phys. Prototyp.* 10 (4) (2015) 195–206, <https://doi.org/10.1080/17452759.2015.1112412>.
- [186] A. du Plessis et al., *3D Print. Addit. Manuf.* 5 (3) (2018) 227–247, <https://doi.org/10.1089/3dp.2018.0060>.
- [187] C. Qiu, N.J.E. Adkins, M.M. Attallah, *Mater. Sci. Eng., A* 578 (2013) 230–239, <https://doi.org/10.1016/j.msea.2013.04.099>.
- [188] D. Buchbinder et al., *J. Laser Appl.* 26 (1) (2014) 012004, <https://doi.org/10.2351/1.4828755>.
- [189] C. Zhong et al., *Opt. Laser Technol.* 75 (2015) 87–92, <https://doi.org/10.1016/j.optlastec.2015.06.016>.
- [190] H. Atkinson, S. Davies, *Metall. Mater. Trans. A* 31 (2000) 2981–3000, <https://doi.org/10.1007/s11661-000-0078-2>.
- [191] W.J. Sames et al., *Int. Mater. Rev.* 61 (2016) 315–360, <https://doi.org/10.1080/09506608.2015.1116649>.
- [192] H.L. Wei et al., *Prog. Mater Sci.* 116 (2021) 100703, <https://doi.org/10.1016/j.pmatsci.2020.100703>.
- [193] S. Kou, *JOM* 55 (6) (2003) 37–42, <https://doi.org/10.1007/s11837-003-0137-4>.
- [194] F. Brückner, C. Leyens, **Hybrid laser manufacturing**, in: M. Brandt (Ed.), *Laser Additive Manufacturing: Materials, Design, Technologies, and Applications*, Elsevier, 2017, pp. 79–97. Ch. 3, <http://dx.doi.org/10.1016/B978-0-08-100433-3.00003-8>.
- [195] S.A. Khairallah et al., *Acta Mater.* 108 (2016) 36–45, <https://doi.org/10.1016/j.actamat.2016.02.014>.
- [196] E. Yasa et al., *Procedia CIRP* 45 (2016) 175–178, <https://doi.org/10.1016/j.procir.2016.02.068>.
- [197] C. Qiu et al., *Acta Mater.* 96 (2015) 72–79, <https://doi.org/10.1016/j.actamat.2015.06.004>.
- [198] H. Masuo et al., *Procedia Struct. Integrity* 7 (2017) 19–26, <https://doi.org/10.1016/j.prostr.2017.11.055>.
- [199] W. Jin et al., *Appl. Sci.* 10 (2020) 1563, <https://doi.org/10.3390/app10051563>.
- [200] B. Wu et al., *J. Manuf. Processes* 35 (2018) 127–139, <https://doi.org/10.1016/j.jmapro.2018.08.001>.
- [201] S. Thapliyal, *Mater. Res. Express* 6 (2019), <https://doi.org/10.1088/2053-1591/ab4dd4>.
- [202] D. Deng, H. Murakawa, *Comput. Mater. Sci.* 43 (4) (2008) 591–607, <https://doi.org/10.1016/j.commatsci.2008.01.003>.
- [203] Y. Lee et al., *Appl. Sci.* 9 (2019) 5115.
- [204] K. Stenberg et al., *J. Mater. Res.* 33 (14) (2018) 2077–2086, <https://doi.org/10.1557/jmr.2018.234>.
- [205] S. Bose, S.F. Robertson, A. Bandyopadhyay, *Acta Biomater.* 66 (2018) 6–22, <https://doi.org/10.1016/j.actbio.2017.11.003>.
- [206] V.K. Balla, S. Bose, A. Bandyopadhyay, *Int. J. Appl. Ceram. Technol.* 5 (3) (2008) 234–242, <https://doi.org/10.1111/j.1744-7402.2008.02202.x>.
- [207] V. Krishna Balla et al., *Rapid Prototyp. J.* 18 (6) (2012) 451–457, <https://doi.org/10.1108/13552541211271992>.